Cardiovascular Image-Derived Phenotypes from Abdominal MRI at a Population Scale

Nicolas Basty[1*], Elena P. Sorokin[2*], Marjola Thanaj[1], Brandon Whitcher[1], Yi Liu[2], Jimmy D. Bell[1], E. Louise Thomas[1*], Madeleine Cule[2*]

[1] Research Centre for Optimal Health, School of Life Sciences, University of Westminster, London, UK
[2] Calico Life Sciences LLC, South San Francisco, California, USA
* contributed equally
correspondence: n.basty@westminster.ac.uk, cule@calicolabs.com

Abstract

MRI measurements of heart volumes and vessel dimensions typically require specialised cardiac MRI examinations, which can be time consuming and resource intensive. Simpler scans covering the heart and major blood vessels of the abdomen may potentially provide useful clinical information. We used deep learning to segment cardiovascular structures from UK Biobank abdominal MRI scans and extracted six image-derived phenotypes (heart volume, and cross-sectional areas of the aorta and vena cava at key anatomical locations) from 44,541 participants. We found strong correlations between our measurements and those acquired using conventional cardiac MRI (CMR), with the strength of the association reflecting the degree of anatomical similarity between the measurements. We replicated previous findings related to sex differences and age-related changes in heart and vessel dimensions, and identified a significant association between infrarenal descending aorta cross-sectional area and incident aneurysm, and between heart volume and several cardiovascular disorders. In a genome-wide association study we identified 72 associations at 59 loci, of which 15 had not been previously associated with CMR image-derived phenotypes. Furthermore, we demonstrated substantial genetic correlation with cardiovascular traits including varicose veins, aneurysms, dysrhythmia and cardiac failure. Our heritability enrichment implicated vascular tissue in the heritability of these traits. We derived a polygenic risk score for each trait and demonstrated an association with aneurysm diagnosis, pointing to a potential screening method for individuals at high-risk of this condition. Our work highlights the rich information content of abdominal MRI and the high degree of overlap with CMR.

Keywords: Whole-body MRI, Segmentation, Deep learning, GWAS, Cross-Sectional Area, Aorta, Aneurysm

Introduction

Cardiac MRI (CMR) is considered the gold standard for cardiovascular image-derived phenotypes (IDPs) including ventricular volumes, wall thickness and ejection fraction, each

of which has an established relationship to cardiovascular disease risk.[1] These scans are expensive and time-consuming to acquire, and do not capture information about blood vessels further away from the heart. The feasibility of measuring aorta diameters using non-cardiac MRI acquisitions has been shown by Mensel et al.[2], where strong correlations between measurements from cardiac and non-cardiac sequences were established. Recently it has been shown that cardiovascular risk factors can be predicted based on visible blood vessels in retinal photographs.[3] Similarly, repurposed chest X-rays have been used to detect early heart failure[4], highlighting the potential added value in clinical images beyond their primary purpose. While not sharply defined due to cardiac motion, the heart, aorta and vena cava are all discernible in the UK Biobank (UKBB) abdominal MRI data. (**Figure 1A**). We hypothesise that meaningful cardiovascular measurements can be extracted from UKBB abdominal MRI, and that these measurements may provide new insights into the etiology of a range of cardiovascular disease outcomes including the detection of abdominal aortic aneurysm (AAA) during routine clinical investigations, a condition that continues to be a significant cause of clinical complications and death.[5,6]

Previous studies have demonstrated that CMR IDPs in the UKBB, including diameter of the ascending and descending aorta[7] and ventricular volumes,[8] have a substantial heritable component. The cross-sectional areas (CSAs) of vessels represent different partitions in the body receiving blood supply and their sizes are associated with variation in blood supply, blood pressure, age and body size.[9] Average heart volume can be seen as a surrogate for cardiac structure in an analogous fashion to BMI being a commonly used estimate of body composition, despite its recognised limitations. We have applied our methodology to 44,541 abdominal scans from UKBB participants and conducted genome, exome and phenome-wide association studies to identify genetic and lifestyle factors contributing to variability in the cardiovascular IDPs.

Results

Population-scale inference of cardiovascular IDPs from abdominal MRI

We extracted a total of six IDPs from the neck-to-knee MRI acquisitions (n=44,451) (**Figure 1A**), volume of the heart, and CSAs of the aortic arch, descending aorta (thoracic, suprarenal, infrarenal) and superior vena cava (**Figure 1B)**. On average, men had higher values than women for all IDPs (**Figure 2A, ST1 and ST2**). After adjusting for sex, imaging centre, scan date, and scan time, vascular CSAs were positively associated with age, with aortic arch increasing at 5.63mm^2/year in men (5.24mm^2/year in women), thoracic descending aorta at 4.53mm^2/year in men (3.93mm^2/year in women), and suprarenal descending aorta increasing at 3.85mm^2/year in men (3.60mm^2/year in women) (**Figure 2B**; **ST3**).

In order to assess the relationship between our IDPs and related measures derived from CMR, we computed the correlation between our cardiovascular abdominal IDPs and the IDPs derived from CMR in the same cohort[10]. Heart volume was positively correlated with both atrial and ventricular volumes and the diameters of the ascending and descending

aorta, and negatively correlated with ventricular ejection fractions. In the aorta, the strongest correlation was between the CMR descending aorta and abdominal thoracic descending aorta, with progressively weaker correlation for landmarks further down the abdominal aorta (**Figure 2C**).

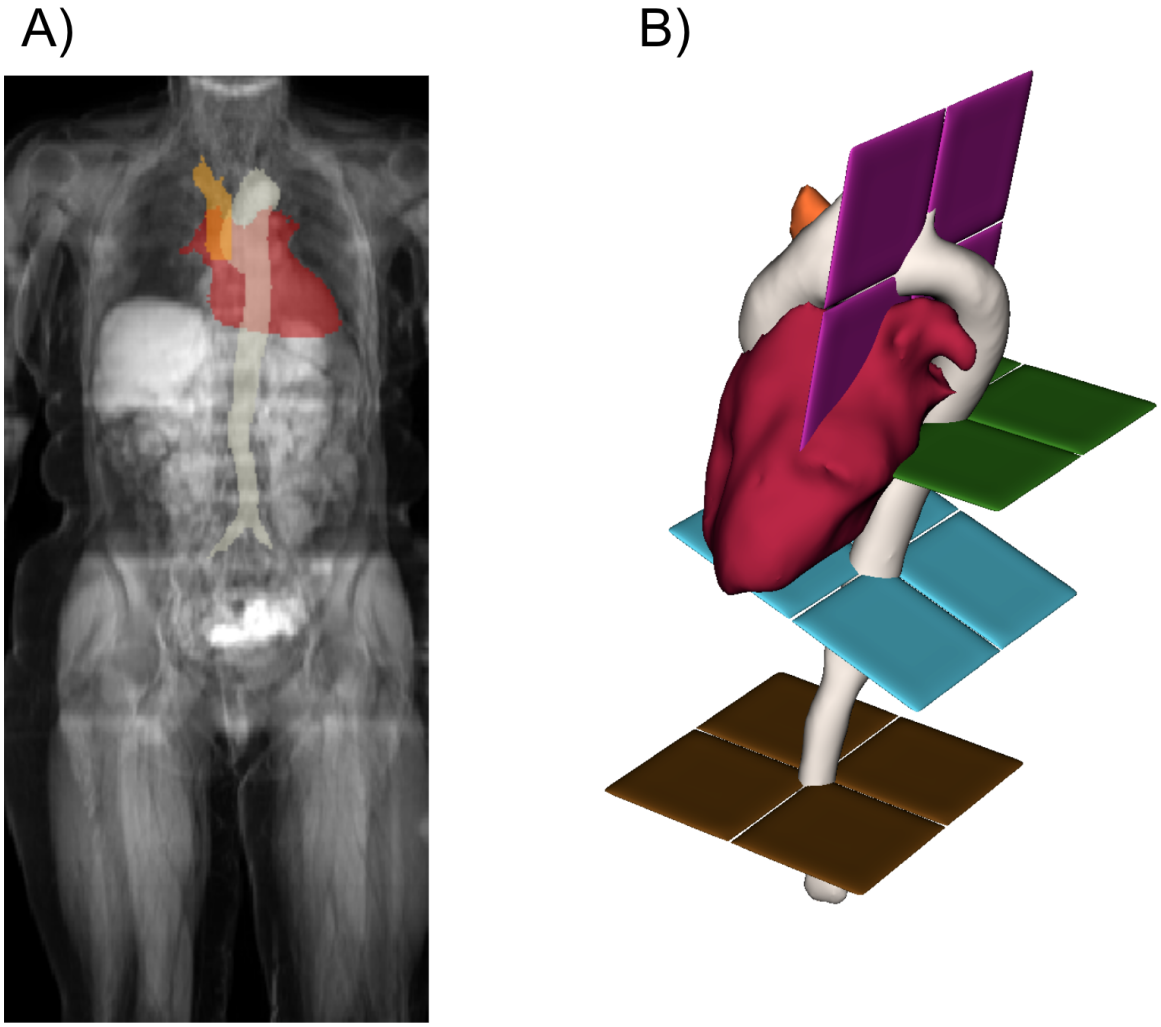

Figure 1: Graphical representation of cardiovascular IDPs from abdominal MRI. A: Planar projection coronal view of Dixon MRI data superimposed with planar projections of 3D segmentations: aorta (white), vena cava (orange), heart (red). **B:** 3D segmentations: aorta, vena cava, heart, orthogonal planes to extract cross-sectional areas at aortic arch (pink), thoracic descending aorta (green), suprarenal aorta (blue), infrarenal aorta (brown).

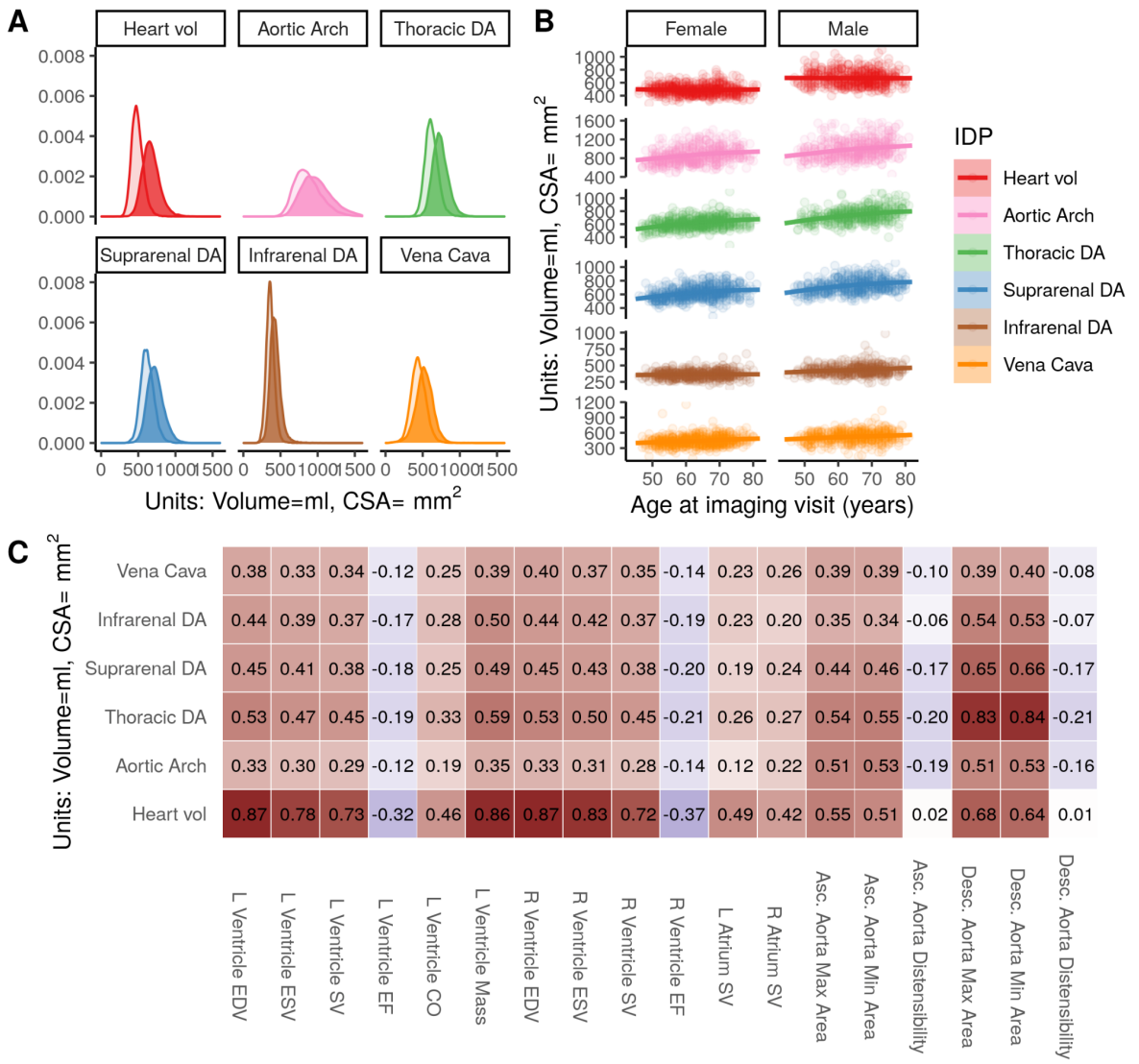

Figure 2 Summary of Image-derived phenotypes. A: Distributions of six IDPs: heart (volume), aortic arch CSA, thoracic descending aorta CSA, suprarenal descending aorta CSA, infrarenal descending aorta CSA, and superior vena cava CSA. Women: transparent colours, Men: solid colours. **B:** Cardiovascular IDP relationships with age and sex. **C:** Correlations between our IDPs and those obtained from CMR.[10] CSA=cross-sectional area, DA=Descending Aorta, EDV=End Diastolic volume, ESV=End systolic volume, SV=Stroke volume, EF=Ejection fraction, CO=Cardiac output.

Phenome-wide association study links vascular IDPs with cardiovascular disease outcomes and quantitative traits

To explore the relation between abdominal IDPs and a range of disease outcomes, lifestyle factors, and quantitative traits, we conducted a phenome-wide association study across approximately 1500 disease PheCodes[11] (**Figure 3A, ST4**), and approximately 2500 lifestyle factors, self reported outcomes and quantitative traits (**ST5, SF1-5**). Heart volume was correlated with multiple cardiovascular outcomes including cardiomyopathy, valve disorders, heart failure, angina and dysrhythmias. Type 2 diabetes (T2D) was associated with lower

heart volume and smaller CSA in all of the vessels measured. In addition, we found an association between aortic arch CSA and hypertension, between suprarenal descending aorta and vena cava CSA and varicose veins and between infrarenal descending aorta CSA and aneurysms.

We also explored the extent to which our IDPs could act as a prognostic biomarker for future major adverse cardiac events (MACE), aneurysm and varicose vein diagnoses (**Figure 3B**). After adjustment for age, sex, height, and weight. Infrarenal aorta CSA was a risk factor for incident aneurysm diagnosis (hazard ratio 1.835, 95% confidence interval [1.595-2.105]), while increased heart volume was a risk factor for MACE (hazard ratio 1.444 [1.328-1.569]) and varicose veins (hazard ratio 1.337 [1.002-1.783]). No other IDPs were significantly associated with incident disease, although due to the limited follow-up period from the imaging visit, our power to detect associations is limited.

We selected two thresholds for infrarenal aortic aneurysm, and evaluated how many participants with this threshold received a diagnosis of AAA. The first threshold was derived from the literature suggesting a diagnosis of aneurysm of infrarenal CSA>700mm^2 (3cm diameter)[12] a CSA>2SD above the mean (**ST6**) (for men CSA>652.44mm^2 (2.88cm diameter); for women CSA>509.75mm^2 (2.55cm diameter)). Most individuals with a diagnosis of aneurysm had a CSA dimension below than the 3cm threshold (110 of 126 men and 6 of 7 women cases) at the time of scanning. **Figure 3C** shows the distribution of infrarenal aorta CSAs by sex and aneurysm diagnosis status, and diagnostic threshold of infrarenal CSA>700mm^2.

Heart volume and aortic CSAs were associated with alcohol consumption (**SF1, ST5**). Heart volume, aortic CSAs at all locations, and vena cava CSA were positively associated with physical activity (**SF2, ST5**), consistent with the negative association with T2D. Larger heart volume was associated with greater self-reported satisfaction with health, lower anxiety, and decreased lethargy, as well as reduced self-reported digestive problems such as sensitive stomach, digestive pains, and difficulty with bowel movements.

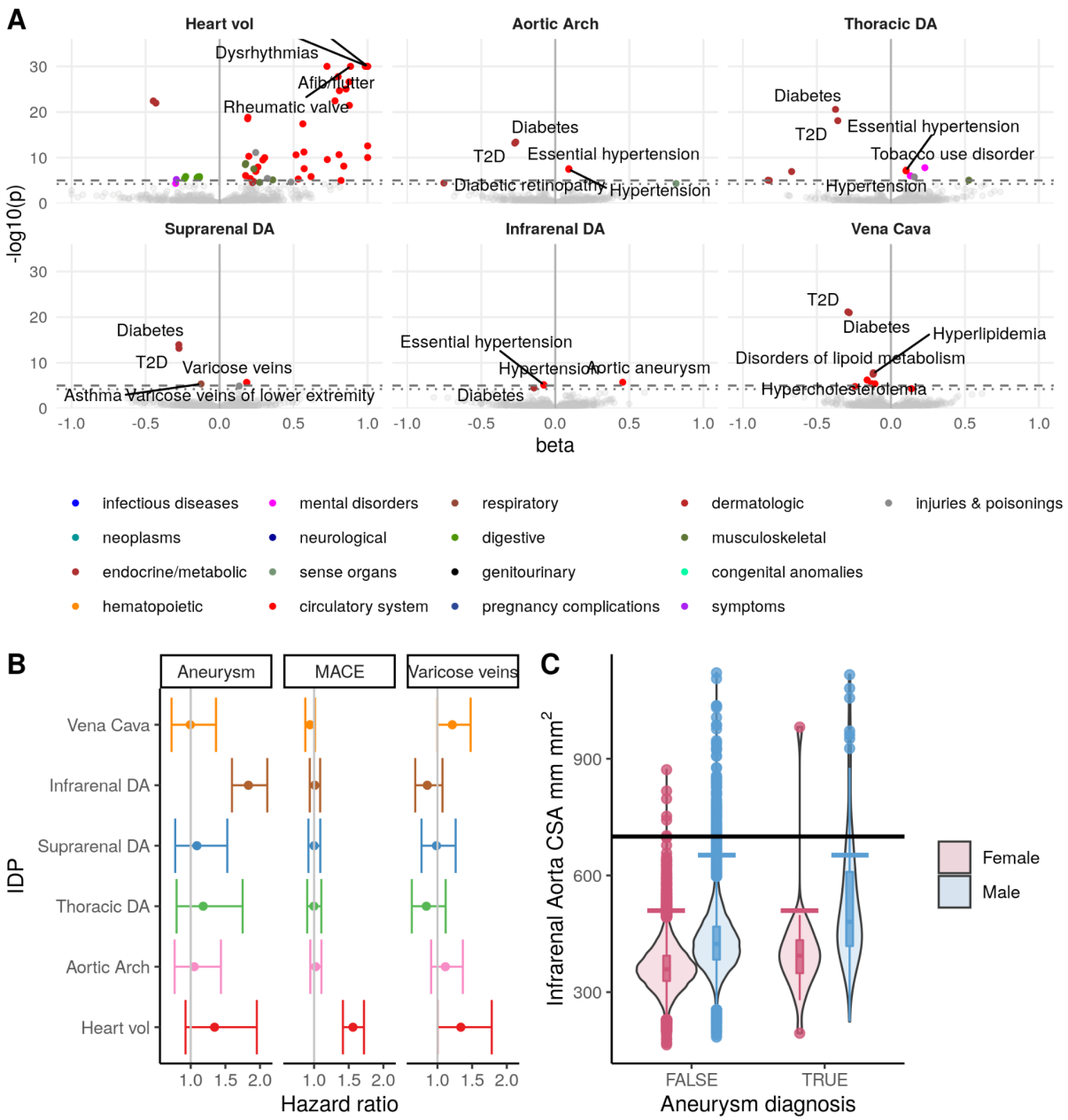

Figure 3 A: Disease phenome associations between cardiac IDPs and disease phecodes defined based on hospitalization records. T2D = type 2 diabetes. The x-axis is limited to [-1, 1]. **B**: Forest plots of disease survival models for Aneurysm, Major adverse cardiovascular events (MACE) and varicose veins. Bars represent 95% confidence intervals. **C**: Violin plots for infrarenal aorta CSA and aneurysm diagnosis status. The black horizontal line is a literature suggested threshold for aneurysm. The horizontal segments represent two standard deviations above the mean CSA, 652.44mm^2 CSA for men and 509.75mm^2 CSA for women.

Genome-wide association study identifies 59 loci associated with vascular IDPs

To explore the genetic contribution to variability in the six IDPs, we conducted a genome-wide association study (GWAS) in approximately 35,000 individuals of White British ancestry (**ST1**). SNP-heritability of the CSAs ranged from 17%-42%, with heritability of the

heart volume estimated to be 45% (**ST7**), confirming that vascular IDPs have a substantial heritable component.

We identified a total of 59 loci associated with at least one trait at genome-wide significance ($p<5e-8$) (**Figure 4A, ST8**). Seven loci were associated with multiple traits. We identified associations at a total of 72 trait-locus pairs, of which 44 reached study-wide Bonferroni-corrected significance threshold ($p<8e-9$). With one exception, where two traits both shared a signal at the same locus, a colocalisation test revealed that the two traits likely shared the same lead SNP. The exception to this is the *PLCE1* locus, where we identified a total of four independent signals with different patterns of sharing between aortic arch, thoracic descending aorta, and suprarenal descending aorta. A conditional analysis revealed no secondary signals at any locus except *PLCE1*.

To explore the extent to which the genetic basis of our traits are shared with CMR traits, cardiovascular disease outcomes, and relevant quantitative traits more broadly, we estimated the genetic correlation between our IDPs and other traits and disease outcomes (**Figure 4B-C** and **SF8**). We observed that the CMR-based descending aorta diameter has the strongest genetic correlation (r_g=0.91) with thoracic descending aorta CSA, and weaker correlation with CSA measures lower in the abdomen. The ascending aorta diameter has the strongest correlation with aortic arch CSA (r_g=0.77). Heart volume from abdominal MRI shows positive genetic correlation with left ventricular end systolic and diastolic volume and with stroke volume, and negative genetic correlation with left ventricular ejection fraction. We found evidence for genetic correlation between aneurysms and vessel CSA (especially suprarenal descending aorta, r_g=0.87), and between varicose veins and vessel CSA (especially vena cava, r_g=0.37). There was limited evidence for a genetic correlation between vessel CSA and other cardiovascular traits such as pulse pressure, ischaemic heart disease, and coronary artery disease (**Figure 4C** and **SF7**).

To explore which tissues or cell types were responsible for the heritability of these traits, beyond identifying tissue-specific eQTLs, we used stratified LD score regression[13] to partition the heritability of each trait across regions defined by cell-type-specific chromatin marks. After Bonferroni correction for multiple hypothesis testing, we identified enrichment in cardiovascular cell types including aorta and fetal heart for all of the traits except vena cava CSA **(Figure 5A**). We also applied the same methodology using annotations based on tissue-specific gene expression.[14] This did not yield significant enrichment in any tissue (**SF9**).

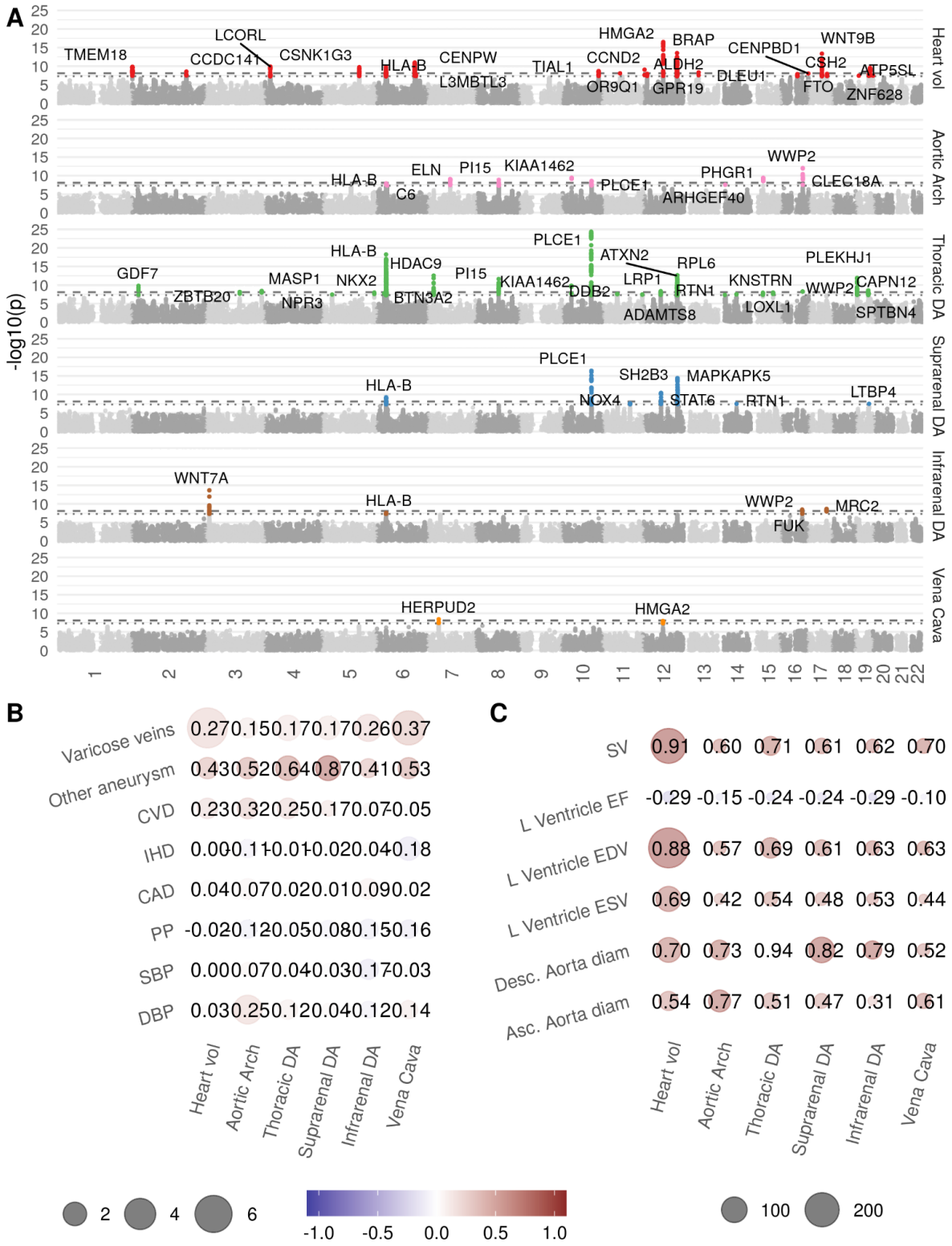

Figure 4A: Manhattan plot for the one volume and five CSA traits. Dotted line: single-trait significance threshold of 5e-8. Dashed line: study-wide significance threshold of 8e-9. Loci reaching study-wide significant locus is labelled with the closest gene (defined by distance between the lead SNP and the transcription start site). **B**: Genetic correlation between cardiac IDPs and cardiovascular complex traits. CAD: Coronary artery disease. PP: Pulse

pressure. SBP: Systolic blood pressure. DBP: Diastolic blood pressure. Size of the points are -log10(p) of the genetic correlation. Color is genetic correlation. **C**: Genetic correlation between cardiac IDPs and measures derived from CMR. SV: Stroke volume. ESV: End systolic volume. EF: Ejection fraction. EDV: End diastolic volume.

To identify loci where the effect on the phenotype may be mediated by changes in expression, we conducted a colocalisation analysis with expression data from five vascular tissues obtained from GTEx version 7 (artery - aorta, artery - tibial, artery - coronal, heart - atrial appendage, and heart - left ventricle (**Figure 5B** and **ST9**). We identified 31 genes with some evidence (posterior probability > 0.7) of colocalisation of an eQTL in at least one vascular tissue with at least one IDP, with several showing evidence for association in multiple tissues or with multiple IDPs. For example, a locus overlapping *LRP1* and *STAT6* is associated with suprarenal descending aorta (10 SNPs in credible set) and thoracic descending aorta (25 SNPs in credible set). Both signals colocalise with changes in *LRP1* expression in both tibial and aortic arteries. *LRP1* is an endocytic and signalling receptor with an established role in protection from aneurysms.[15]

Of the 72 trait-locus pairs, 47 show evidence (PP4 > 0.9) of a shared signal with at least one CMR IDP (**SF6**). In particular, 20 of the 26 genome-wide-significant loci associated with the thoracic descending aorta were previously reported in a study of CMR-derived descending aorta[8], and 12 and nine heart volume loci were reported in LV-ESV and LV-SV, respectively (**SF6**). This reflects the physiological basis of the traits, despite the fact that different acquisition protocols were used. Several loci have been implicated in previous studies of cardiovascular traits and outcomes (**SF7**).

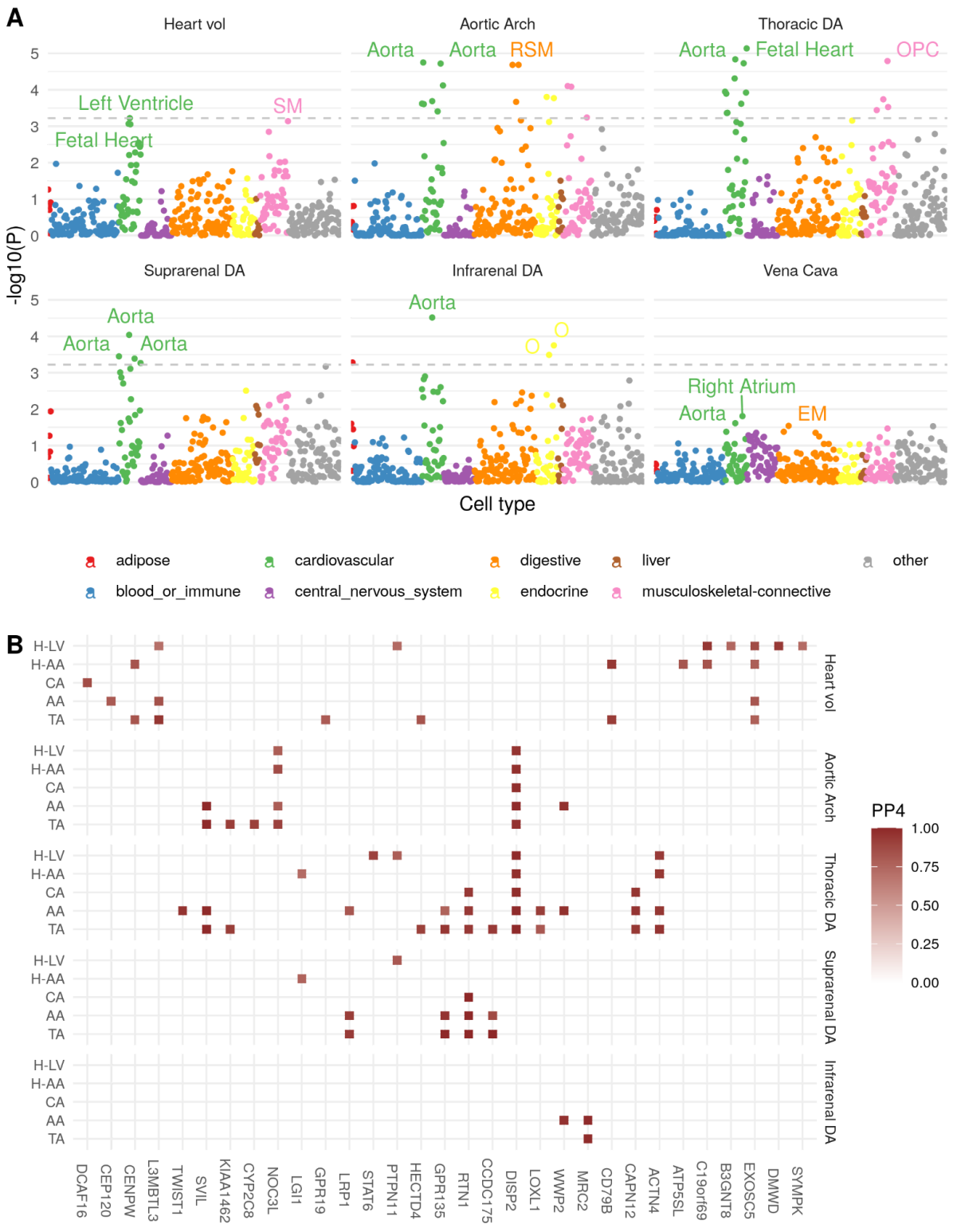

Figure 5A: Heritability Enrichment. Dashed horizontal line at FDR of 0.05. Y-axis: P-value of the coefficient of the annotated tissue in a model adjusting for baseline genome features. The top three tissue or cell types are labeled for each IDP. Abbreviations: EM:esophagus muscularis, O:ovary, OPC:osteoblast primary cells SM:skeletal muscle. **B**: Colocalisation probabilities associated with changes in gene expression in cardiovascular tissues in GTEx version 7. Abbreviations for tissues: H-LV heart left ventricle, H-AA heart atrial appendage,

CA coronary artery, AA aortic artery, TA tibial artery. Colocalisations with PP4 > 0.7 are colored. Genes are ordered according to chromosomal location.

Polygenic risk scores are associated with cardiovascular disease outcomes and survival time

To examine whether the polygenic effect of abdominal IDPs was associated with relevant clinical outcomes, we constructed polygenic scores (PRS) for each IDP **(SF12)**. Using a validation set of European ancestry individuals in the UKBB without imaging data (n=250,753), we assessed associations of these scores across the medical phenome. Across IDPs, the significant associations (FDR<0.01) were enriched for positive associations with cardiovascular outcomes. For example, thoracic descending aorta PRS was associated with other aneurysms (p=1.0e-7), cardiac dysrhythmias (p=7.3e-7), and hypertension (p=1.1e-6); heart volume PRS was associated with cardiac dysrhythmias (p=3.8e-10) and hypertension (3.2e-6); and vena cava PRS was associated with ischemic heart disease (p=1.7e-5) (**ST10**).

We probed whether PRS were associated with time to event for several acute cardiovascular events: aortic aneurysm, myocardial infarction, and stroke. We found that PRS were associated with time to event for first aortic aneurysm for the thoracic descending aorta (HR=1.11 per SD increase in PRS, p=7.3e-7), aortic arch (HR=1.09, p = 9.7e-5), suprarenal descending aorta (HR=1.08 per SD increase in score, p = 3.1e-4), infrarenal descending aorta (HR=1.06, p = 4.6e-3), and heart volume (HR=1.07, p = 1.1e-3) (**ST11**). None of the associations with time to first diagnosis of hypertension, myocardial infarction event, or stroke event were significant (FDR < 0.01) (**ST11**). Kaplan-Meier curves for aortic aneurysm event-free survival, stratified by polygenic risk scores for these cardiovascular six traits, among the top 2.5%, middle 95%, and bottom 2.5% of each risk score distribution, show there is a strong relationship between these cardiovascular IDPs and time to first aortic aneurysm event (**Figure 6**).

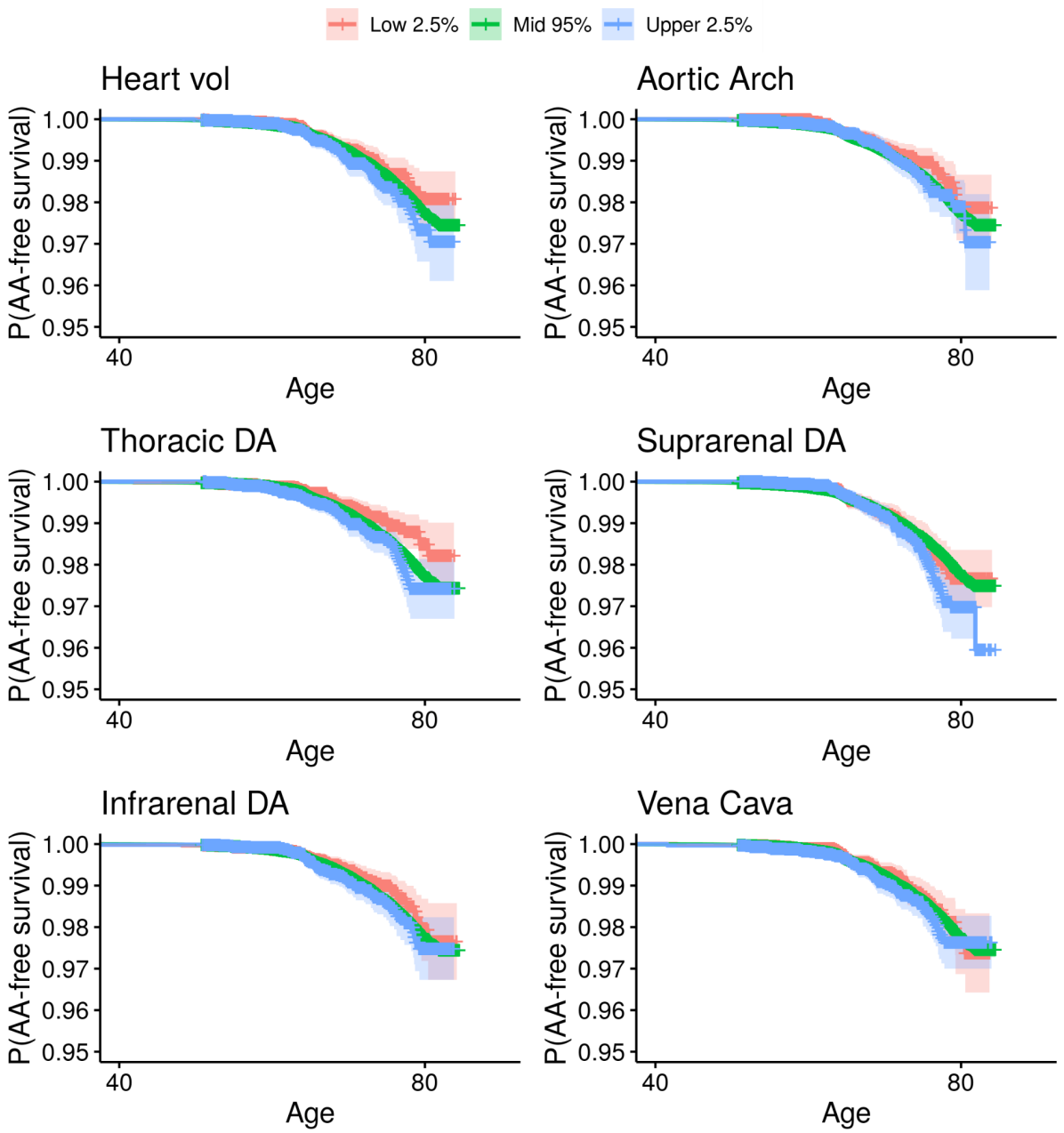

Figure 6: Kaplan-Meier curves for first aortic aneurysm diagnosis in the UK Biobank, stratified by polygenic risk score percentile. Polygenic risk scores are stratified by percentile (red: bottom 2.5% , green: middle 95%, blue: top 2.5%) for each of six IDPs: **A:** heart (volume), **B:** aortic arch (cross-sectional area, or CSA), **C:** thoracic descending aorta CSA, **D:** suprarenal descending aorta CSA, **E:** infrarenal descending aorta CSA, and **F:** superior vena cava CSA. Y-axis, event-free probability for first recorded aortic aneurysm. X-axis, age of participant (years) at time of first event. Shaded areas represent confidence intervals.

Exome-wide rare variant association study links loss-of-function of a Wnt ligand with heart volume

To investigate the contribution of rare loss-of-function variation and to identify other potential genes associated with cardiovascular IDPs, we performed rare variant association studies using putative loss-of-function mutations and a combined burden and SKAT test. The only

association significant after multiple testing was between loss-of-function variants in *WNT10B* and heart volume (**SF10)**. *WNT10B* is a member of the WNT family of signalling proteins and has been implicated in post-injury cardiac repair.[16]

Discussion

In this study we repurposed UKBB abdominal MRI and measured cross-sectional areas (CSAs) of the aortic arch, descending aorta (thoracic, suprarenal, infrarenal), and superior vena cava. We also measured total heart volume. Deep learning was used to segment 3D structures from the images and extract 2D planes at relevant landmarks to quantify the vasculature. We explored how these results compare with cardiac measurements made by conventional CMR and provided in-depth phenotypic and genetic analyses.

We found strong correlations between our opportunistic measures of heart volume and conventional measures of ventricular mass, diastolic and systolic volume, and stroke volume. This was somewhat surprising since our heart volume measurements were acquired without cardiac gating. Similarly, there were statistically significant correlations between our opportunistically measured aortic and vena cava CSAs with minimal and maximal measures of ascending and descending aorta area measured by CMR. The strongest association was observed for the thoracic descending aorta, which is perhaps to be expected since this measurement closely corresponds to the location of CMR measurements of the ascending and descending aorta.[10]

In agreement with previous studies, our measurements were significantly larger in men than women,[10,17,18] with increased aortic diameter in men suggested as a reason for the greater incidence of AAA in men.[19] We found that CSA IDPs increased with advancing age, in both men and women. Aortic diameter has been previously shown to increase with age[20], accompanied by a concomitant decrease in aortic distensibility.[10] Previous studies have suggested that abdominal aortic diameter may increase by as much as 30% between the ages of 25 and 71 years.[21] We found similar increases in both men and women (**Figure 2B**, **ST3**). We have previously shown in a longitudinal analysis of a smaller subset of 3,088 UKBB participants, who were scanned a second time approximately 2.5 years after their baseline scan, that aortic CSA values significantly increased.[22] However, the magnitude of the increases we have observed from cross-sectional compared with our longitudinal observations varies, for instance after 2.5 years, the infrarenal aorta CSA increased by approximately 4.0mm^2 in women and 6.1mm^2 in men, with the per-year changes over the same period predicted to be 0.7mm^2 in women and 4.0 mm^2 in men. This suggests that cross-sectional measurements may underestimate age-related longitudinal changes. However, it is important to remember that these changes are small in magnitude and may be impacted by measurement errors.

CMR enables precise measurements of specific regional measures such as ventricular volumes and hence there is little focus on the whole heart. However, total heart volume has been found to determine the extent of volumetric change during the cardiac cycle.[23,24] This is estimated to be between 5-8% and presumed to be related to changes in total blood volume rather than cardiac muscle mass. Given the relatively long acquisition time and lack of

cardiac gating, the heart will be the average of several beats in our data. Nevertheless, we showed that larger heart volume was strongly associated with cardiovascular disease, whereas reduced heart volume was associated with T2D. This is an unexpected finding since T2D has typically been associated with increased left ventricular mass (LVM).[25] It has been suggested that this may be more of a reflection in the association between overweight/obesity commonly reported in T2D instead of an association between T2D and LVM specifically, however studies controlling for body mass have confirmed the same observation.[26] A recent study using CT-based whole heart volume found that smaller volumes were more common in individuals with diabetes.[27] These seemingly contradictory results may be explained by differences in their respective methodological approaches, however Foldyna et al.[27] made the interesting observation that there appeared to be a J-shaped curve between heart volume and MACE, with smaller volumes associated with non-obstructive coronary artery disease (CAD) and larger volumes associated with obstructive CAD. Indeed, we found larger heart volume to be associated with physical activity and other self-reported indicators of health. Taken together, this indicates that larger heart volumes can reflect either cardiovascular health (lower risk of metabolic disease, lower heart rate, higher self-reported satisfaction) or increased cardiovascular risk (higher risk of atrial fibrillation, rheumatic heart disease, or cardiomyopathy), with more precise measurements needed to distinguish between these factors.

We found associations between vasculature and disease, with smaller CSAs in all vessels measured associated with T2D. This agrees with the prevailing literature[28], which is thought to be a factor in the reduced incidence of aneurysms in people with T2D.[29] We also found a significant association between infrarenal descending aorta and aneurysm in a time-to-event model, but our measurements in other aortic regions were not significantly associated. This is significant given the infrarenal portion of the aorta is the most common location for AAA, with evidence that increased diameter of the infrarenal aorta is an independent risk factor for AAA.[19] Interestingly, despite the sex differences in aorta CSA, thresholds for defining elevated aortic diameter, and therefore increased risk of AAA, are not currently sex-specific. For example, a definition at infrarenal aorta given as diameter >3cm[12,30], while others suggest individuals with an aortic diameter >2.6 cm should be regularly screened for AAA.[19] 144 men and 24 women were diagnosed with AAA. Using the >3cm (700mm^2) threshold we identified 126 men and 7 women who would have been classified as having AAA. However, only 11% of men and 4% of women with a diagnosis of aneurysm exceeded this threshold. We determined a different sex-specific threshold calculated from +2SD of the infrarenal CSA (men 652.44 mm^2 or 2.88 cm; and women 509.75 mm^2 or 2.55 cm), and identified 5.5 times more men and 10 times more women potentially at risk of AAA, compared to the 3cm cut-off. However, this threshold had low specificity and sensitivity for diagnosis with aneurysm. This may reflect changes since the time of scanning, or differences in the location of the aneurysm. The low overlap of diagnosed cases and increased CSA measurements could also be a sign of the fact that this is an often underdiagnosed condition.[31] A study by MacDonald et al.[32] showed 77% of patients in their retrospective analysis were not diagnosed with AAA before rupture, although 76% of them had attended a medical facility in the five preceding years, underlining the fact that AAA are often missed. The authors encourage opportunistic screening of patients attending hospital regardless of the reason for their visit, and automated methods like ours could facilitate this endeavour. Longitudinal

measurements and relevant outcome data will be required to evaluate whether aortic diameter alone is a clinically useful measure in screening for aneurysm risk.

Our genome-wide association study confirms that, like CMR IDPs, cardiovascular abdominal IDPs have a substantial heritable component. We identified 72 associations at 59 loci; of these 47 had previously been associated with a CMR IDP, with the remainder being newly identified. We demonstrated substantial genetic correlation with cardiovascular traits including vascular disorders such as varicose veins and aneurysm, as well as cardiac dysfunction such as dysrhythmia and cardiac failure. At several of these loci, we could implicate potential causal genes by integration with expression QTL data in relevant tissues. Our heritability enrichment implicated vascular tissue in the heritability of these traits. We derived a polygenic risk score for each trait and demonstrated a novel association with aneurysm diagnosis, pointing to a potential screening method for individuals at high-risk of this condition.

While our exome-wide association study was limited in power due to sample size, we identified an association between heart volume and *WNT10B,* a Wnt signaling ligand which is expressed in cardiac and skeletal muscle[33], which has a known role in cardiac formation during development and in positive response to injury in adulthood.[16]

This study has some limitations. The images have relatively low resolution, especially compared to dedicated CMR, hence vessels have insufficient detail to differentiate between the wall and lumen. Furthermore, heart volumes are subject to measurement error depending on where the neural networks differentiated between vasculature and the heart. Despite this we found a very high correlation between CMR and our cardiovascular abdominal IDPs, confirmed many of the genetic findings arising from CMR as well as identified novel hits. The UKBB imaging cohort is healthier than the wider UK population[34], predominantly white, and does not include participants under the age of 40, meaning our findings may not be easily extrapolated to different populations or age categories.Our study has a relatively limited follow-up period since the imaging visit (3 years), which limits the power of our time-to-event studies. In our genetic study, which has a longer follow-up since the risk is present from birth, data prior to the widespread adoption of electronic medical records in 1997 is less complete, relying for this period in self-report data collected during participant visits.

By opportunistically repurposing the UKBB abdominal MRI data, we have shown that non-specialised scans may be used to extract meaningful cardiovascular measures enabling genetic analysis of the aorta beyond the field of view provided in CMR, while also highlighting the untapped screening potential of routinely acquired medical images. Despite advances in the early detection and treatment of AAA, rates remain high and continue to increase in many countries. Repurposing images which are routinely collected for clinical investigations to detect an enlarged aorta may provide a useful adjunct to on-going screening programmes and a valuable tool in the majority of countries where screening is not possible. Furthermore, our data suggests that conventional thresholds for aneurysm detection in women need closer inspection and re-evaluation as it could be among the reasons for aneurysms being less frequently observed, but more serious, in women.

Additional clinical work is required to establish more precise thresholds for aneurysms in men and women. Our work adds to the increasing literature on extracting value from images initially acquired for different purposes, but routine scan screening will need further validation in larger case cohorts and could be extended to other commonly used imaging modalities such as ultrasound, DXA and CT.

Methods

Data

Participant data was obtained through UK Biobank Access Application number 44584. The UK Biobank has approval from the North West Multi-Centre Research Ethics Committee (REC reference: 11/NW/0382). All measurements were obtained under these ethics, adhering to relevant guidelines and regulations, with written informed consent obtained from all participants. Researchers may apply to use the UK Biobank data resource by submitting a health-related research proposal that is in the public interest. More information may be found on the UK Biobank researchers and resource catalogue pages (https://www.ukbiobank.ac.uk).

Image preprocessing and segmentation

Image processing pipelines for the Dixon MRI and standard operating procedures for manual annotations, deep learning for image segmentation, are described in detail in Liu et al.[35] Briefly, we trained a convolutional neural network for 3D segmentation based on the U-net architecture[36] using the neck-to-knee Dixon MRI data as input. For training, we had 109 manual expert annotations of the heart, 101 of the aorta and 101 of the superior vena cava. The Dice similarity coefficients on 20% out-of-sample testing data were 0.88 for the aorta, 0.93 for the heart and 0.82 for the vena cava segmentations. We subtracted vasculature segmentations from the heart segmentation to account for the fact that the segmentations could overlap.

Placing orthogonal planes at relevant landmarks

The aorta may be divided into four segments: the ascending aorta, the descending thoracic aorta, the descending suprarenal aorta, and the descending infrarenal aorta. They each represent different partitions in the body receiving blood supply and their sizes are modulated by variations in blood supply, blood pressure, age and body size.[9] The aorta and the vena cava are tubular structures, and their potential torsion as they progress through the body as well as occasional branches at various locations along the segmentations make extraction of CSAs non-trivial. This problem may be encountered for vasculature, but also other tubular structures such as airways, and others have suggested extraction via orthogonal planes[37], which we have adapted for our purpose. First, we reduced the 3D segmentations to their 1-pixel wide skeletons using the scikit-image function *skeletonize* in Python. A graphical representation of CSA extraction from aorta segmentation is provided in **SF11**, where a planar projection of the lower portion of an aorta segmentation is shown (**A-B**) and its skeleton in pink. For a given landmark, we matched the landmark height

coordinate to that of the skeleton (**SF11A**), and placed a tangent at that pixel to generate an orthogonal plane (**SF11B**). The height of the landmark is shown by a red star (**A**) and the orthogonal plane is shown in orange (**B**). An example of the resulting extracted image plane is shown in **C**, where the aorta CSA is highlighted in orange. For anatomical landmarks, we used the centroid of the heart (thoracic) as well as the top (suprarenal) and bottom (infrarenal) of the kidney segmentations[35] for systematic placement of the different positions of aorta sections. For the aortic arch, the section between the ascending and descending aorta, we chose the highest point of the aorta segmentation. For each landmark we extracted orthogonal planes at adjacent points in the skeleton, to account for the fact that irregularities in the segmentation will result in rough edges in the skeleton that will lead to occasional failures in placing tangents. We calculated a roundness measure (4π * area / 2 * perimeter) and selected the CSA with the largest roundness value closest to the landmark. To calculate the CSA in mm^2, we multiplied the number of pixels in the mask by the axial resolution of the resampled slice, which accounts for the anisotropy of the Dixon MRI acquisition (2.23mm x 2.23mm x 3mm). Quality control included adding an upper threshold at 1600 mm^2 for the aortic arch CSA values. We visually inspected all images, where the threshold was exceeded, to confirm they were failures of the plane placement algorithm. We attribute the failures of the automated extraction at the aortic arch to issues with the segmentation, as in rare cases smaller but significant vessels were connected to the aorta, making skeletonisation and interpretation of the 1D object impossible. As an additional sanity check, we excluded values for which the roundness of the extracted feature was < 0.7.

Phenome-wide association study

We generated a list of variables derived from raw data by using *PHESANT*[38] and removed procedural metrics (e.g., measurement date), duplicates, and raw measures, resulting in a total of 2425 traits. For disease outcomes, we used the R package *PheWAS*[39] to combine ICD10 codes from UKBB Field 41270 into 1,500 distinct phenotype codes or phecodes. We performed linear (quantitative traits) or logistic regression (binary traits) on the 2425 traits and 890 phecodes with at least 20 cases, adjusting for imaging center, date, scan time, age, sex, BMI, height, and ethnicity. We defined two Bonferroni-adjusted p-values: a single-trait value which adjusts for the number of tests in that category, and a study-wide value which additionally adjusts for the number of IDPs in this study. We expect this threshold to be somewhat conservative given the high degree of correlation between traits in this study.

Survival analysis of cardiovascular disease outcomes

Disease outcomes of interest, including aneurysm, major adverse cardiovascular events (MACE) and varicose veins were defined based on the occurrence of ICD10 codes mapped from the various sources, the date of first diagnosis made available as “first occurrence” data (Category 1712) and based on self-reported codes after the baseline imaging visit. The codes for aneurysm were selected based on the ICD10 code for “aortic aneurysm and dissection” and the self-reported codes for “aortic aneurysm" and “aortic aneurysm rupture”. MACE was defined based on the ICD10 codes defined from [40] including “acute myocardial infarction” and self-reported codes for “heart failure/pulmonary edema”, “peripheral vascular disease”, “cardiomyopathy”, “atrial fibrillation”, “heart arrhythmia”, “atrial flutter”, “stroke” and “heart attack/myocardial infarction”. The codes for varicose veins were selected based on

the ICD10 for “varicose veins of lower extremities” and “varicose veins of other sites” and the self-reported codes for “varicose veins”. A full list of the codes corresponding to the disease outcome is provided in **ST12**. Cox proportional hazards models were computed for risk of the disease outcomes that were diagnosed after the baseline imaging visit, adjusted for relevant covariates. Time-to-event was determined as the first event for each outcome, death, or censored at the last recorded follow-up (10th February 2022). Any participant who was diagnosed with the disease outcomes before the baseline imaging visit was excluded. The survival analysis was performed using the R *survival* package[41] with model summaries reported as hazard ratios with 95% confidence intervals.

Genome wide association study

We performed a genome-wide association study using the UKBB imputed genotypes version 3,[42] excluding single nucleotide polymorphisms (SNPs) with minor allele frequency <1% and imputation quality <0.9. We included only participants who self-reported their ancestry as ‘White British’ (as defined using UKBB Field 22006) and who clustered with this group in a principal components analysis.[42] We excluded participants exhibiting sex chromosome aneuploidy, with a discrepancy between genetic and self-reported sex, heterozygosity and missingness outliers, and genotype call rate outliers.[42] We used BOLT-LMM version 2.3.2[43] to fit a linear mixed model to estimate the association between each SNP and the IDPs. To calculate the genotype-relatedness matrix used as a random effect, we followed the recommendation of the BOLT-LMM authors and used an LD-pruned (r2 <0.8) set of 574,316 SNPs extracted from the genotyped SNPs and a leave-one-chromosome-out (LOCO) approach to test association with each SNP. We included age at imaging visit, age squared, sex, imaging centre, scan date, scan time, and genotyping batch as fixed-effect covariates, and genetic relatedness derived from genotyped SNPs as a random effect to control for population structure and relatedness. Before conducting the association study, we normalised the outcome variable by using inverse-rank normalisation after regression on fixed covariates.

LD score regression

We verified that the test statistics showed no overall inflation compared to the expectation by examining the intercept of linkage disequilibrium (LD) score regression (LDSC)[44] (**ST13**). For this analysis and all other analyses using LDSC, we followed the recommendation of the developers and (i) removed variants with imputation quality (info) <0.9 because the info value is correlated with the LD score and could introduce bias, (ii) excluded the major histocompatibility complex (MHC) region due to the complexity of LD structure at this locus (GRCh37::6:28,477,797–33,448,354; see https://www.ncbi.nlm.nih.gov/grc/human/regions/MHC), and (ii) restricted to HapMap3 SNPs.[45]

Statistical fine-mapping

We performed approximate conditional analysis using genome-wide complex trait analysis (GCTA)[46], considering all variants that passed quality control measures and were within 500 kb of a locus index variant. As a reference panel for LD calculations, we used genotypes

from 5,000 UKBB participants[42] that were randomly selected after filtering for unrelated participants of white British ancestry. We excluded the major histocompatibility complex (MHC) region due to the complexity of LD structure at this locus. For each locus, we considered variants with genome-wide evidence of association (Pjoint <10–8) to be conditionally independent. We annotated each independent signal with the nearest known protein-coding gene using the R package *biomaRt*[47], querying the ensemble GRC37 database to obtain gene IDs.

Heritability and heritability enrichment

We estimated the heritability of each trait using restricted maximum likelihood as implemented in BOLT version 2.3.2.[48] To identify relevant tissues and cell types contributing to the heritability of IDPs, we used stratified LD score regression[13,14] to examine enrichment in regions of the genome containing genes specific to particular tissues or cell types. We used two types of annotations to define: (i) regions near genes specifically expressed in a particular tissue/cell type, (i) regions near chromatin marks from cell lines and tissue biopsies of specific cell types. For functional categories, we used the baseline v2.2 annotations provided by the developers (https://data.broadinstitute.org/alkesgroup/LDSCORE). Following the original developers of this method, we calculated tissue-specific enrichments using a model that includes the full baseline annotations as well as annotations derived from (i) chromatin information from the NIH Roadmap Epigenomics[49] and ENCODE[50] projects (including the EN-TEx data subset of ENCODE which matches many of the GTEx tissues, but from different donors), (ii) tissue/cell-type-specific expression markers from GTEx v6p[51] and other datasets.[52,53] For each annotation set, we calculated a false discovery rate using the Storey and Tibshirani procedure as implemented in the R package *qvalue*.[54]

Colocalisation and genetic correlation with disease and complex traits

To identify cardiovascular disease traits potentially sharing the genetic basis with our MRI-derived traits, we downloaded summary statistics for 32 relevant traits including CMR derived traits, disease outcomes identified as correlated with our IDPs, and other cardiovascular health measures. The source of these studies are listed in **ST14.** To identify potentially causal genes at each locus, we downloaded QTL data from GTEx (phs000424.v7.p2) to seek evidence for colocalisation with expression in one of 5 cardiovascular tissues. For both complex traits and gene expression, we performed colocalisation analysis using the *coloc* R package[55] using default priors and all considering variants within 500 kb of the index variant of each signal.

Exome variant QC and annotation

We performed QC on whole-exome sequence data from the UKBB by left-aligning indels and annotating variants with the most recent rs numbers from dbSNP v151 (downloaded from https://www.ncbi.nlm.nih.gov/). We filtered out genotypes below minimum depth of coverage of 7 reads for SNPs and 10 reads for indels, or below a minimum genotyping quality score of 20. We filtered out variants with allelic imbalance below 0.15 for SNPs and 0.20 for indels. We filtered out variants with average depth below 10 reads and average

genotyping quality below a score of 25. We used VEPv100 to select variants meeting loss-of-function criteria, further filtered for rare variants (defined as cohort-specific minor allele frequency <0.001). In total, 441,479 variants in 18,808 genes were included in the analysis with 19,992 individuals.

Rare variant association study

We performed rare variant burden and SKAT testing as implemented in SAIGE-GENE, using a mixed-effects model. A kinship matrix was built in SAIGE from a filtered set of 354,878 genotyped variants (r^2<0.2, minor allele frequency >0.05, Hardy-Weinberg p-value >1e-10, excluding known regions of long-range linkage disequilibrium). The linear mixed model regression equation was as follows:

$$y_i = \alpha + \sum_{i=1}^{8} X_i\beta_i + \sum_{j=1}^{5} PC_j\beta_j + G_i\beta + b_i + \epsilon_i$$

In the model, y_i is an inverse-rank normalized image-derived phenotype, X_i represent age at imaging visit, age^2, chromosomally determined sex expressed as a binary indicator variable, the categorical variable of study center as two dummy variables variables, standardized scan date, and standardized scan time. PC_j represents the first five principal components of European genetic ancestry. G_i represents the allele counts (0,1,2) for q variants in each gene to test. We then performed SKAT and burden tests in SAIGE-GENE[56] and reported both the p-value from SKAT-O, which is a linear combination of burden and SKAT: $Q_{SKAT-O} = (1 - \rho)Q_{SKAT} + \rho Q_{burden}$ where ρ is estimated as previously described.[56] To inform directionality of effect, we reported the betas from the burden test. To avoid unstable results at low sample size, we calculated cumulative minor allele count and thresholded at >=5 minor alleles per gene, including singletons and doubletons. Genomic inflation factor was calculated using the *gap* package[57] and summary statistics were visualized in R using the *ggplot2* package.[58]

Polygenic risk score calculation

We trained polygenic risk scores (PRS) using pruning and thresholding (R^2=0.1 and a range of p-values: 1e-8 to 0.1) in a set of UKBB individuals (n=2,567) not included in GWAS. We then calculated scores in a non-imaging European ancestry cohort with complete covariates (n=250,753) using the optimal p-value threshold. This analysis was repeated for each of six traits: CSA aortic arch, CSA thoracic descending aorta, CSA suprarenal descending aorta, CSA superior vena cava and volume of heart minus vessels. Results were visualized in R using the *ggplot2* package.[58]

Survival modeling with PRS

We associated PRS with time to event data in the UKBB: aortic aneurysm, myocardial infarction, and stroke, taking the first recorded event as survival time. This analysis was performed using UKBB participants of European ancestry (based on genetic analysis and

self-reported ethnicity information), and who were not in the imaging subcohort. Since PRS is conferred at birth, we considered the entire patient history as the follow-up period. The Cox proportional hazard model was adjusted for other factors conferred at birth, genetic sex and the first three principal components of genetic ancestry. PRS values were standardized. Modeling was conducted in R using the *survival* package.[41]

Acknowledgments

This research has been conducted using the UK Biobank Resource under Application Number 44584 and was funded by Calico Life Sciences LLC. We thank Kevin Wright and Nick van Bruggen for feedback on the manuscript.

Competing interests

EPS and MC are employees of Calico Life Sciences LLC. YL is a former employee of Calico Life Sciences LLC. NB, BW, JDB, MT, and ELT have no competing interests.

Data availability

Raw data are available to qualifying researchers via application to the UK Biobank. All derived data will be returned to the UK Biobank upon publication. GWAS summary statistics will be made available upon publication at https://www.ebi.ac.uk/gwas/.

References

1. Petersen, S. E. *et al.* UK Biobank's cardiovascular magnetic resonance protocol. *Journal of Cardiovascular Magnetic Resonance* vol. 18 (2015).
2. Mensel, B. *et al.* Thoracic and abdominal aortic diameters in a general population: MRI-based reference values and association with age and cardiovascular risk factors. *European Radiology* vol. 26 969–978 (2016).
3. Poplin, R. *et al.* Prediction of cardiovascular risk factors from retinal fundus photographs via deep learning. *Nat Biomed Eng* **2**, 158–164 (2018).
4. Celik, A. *et al.* The early diagnostic value of chest X-ray scanning by the help of artificial intelligence in heart failure (ART-IN-HF) : The first outcomes. *Journal of the American College of Cardiology* vol. 79 395 (2022).
5. Wang, Z. *et al.* Burden of Aortic Aneurysm and Its Attributable Risk Factors from 1990 to

2019: An Analysis of the Global Burden of Disease Study 2019. *Frontiers in Cardiovascular Medicine* vol. 9 (2022).

6. Wei, L. *et al.* Global Burden of Aortic Aneurysm and Attributable Risk Factors from 1990 to 2017. *Glob. Heart* **16**, 35 (2021).
7. Pirruccello, J. P. *et al.* Deep learning enables genetic analysis of the human thoracic aorta. *Nat. Genet.* **54**, 40–51 (2021).
8. Pirruccello, J. P. *et al.* Analysis of cardiac magnetic resonance imaging in 36,000 individuals yields genetic insights into dilated cardiomyopathy. *Nat. Commun.* **11**, 2254 (2020).
9. Erbel, R. *et al.* 2014 ESC Guidelines on the diagnosis and treatment of aortic diseases: Document covering acute and chronic aortic diseases of the thoracic and abdominal aorta of the adult. The Task Force for the Diagnosis and Treatment of Aortic Diseases of the European Society of Cardiology (ESC). *Eur. Heart J.* **35**, 2873–2926 (2014).
10. Bai, W. *et al.* A population-based phenome-wide association study of cardiac and aortic structure and function. *Nat. Med.* **26**, 1654–1662 (2020).
11. Denny, J. C. *et al.* PheWAS: demonstrating the feasibility of a phenome-wide scan to discover gene-disease associations. *Bioinformatics* **26**, 1205–1210 (2010).
12. Wang, L. J., Prabhakar, A. M. & Kwolek, C. J. Current status of the treatment of infrarenal abdominal aortic aneurysms. *Cardiovasc Diagn Ther* **8**, S191–S199 (2018).
13. Finucane, H. K. *et al.* Partitioning heritability by functional annotation using genome-wide association summary statistics. *Nat. Genet.* **47**, 1228–1235 (2015).
14. Finucane, H. K. *et al.* Heritability enrichment of specifically expressed genes identifies disease-relevant tissues and cell types. *Nat. Genet.* **50**, 621–629 (2018).
15. Strickland, D. K., Au, D. T., Cunfer, P. & Muratoglu, S. C. Low-density lipoprotein receptor-related protein-1: role in the regulation of vascular integrity. *Arterioscler. Thromb. Vasc. Biol.* **34**, 487–498 (2014).

16. Paik, D. T. *et al.* Wnt10b Gain-of-Function Improves Cardiac Repair by Arteriole Formation and Attenuation of Fibrosis. *Circ. Res.* **117**, 804–816 (2015).
17. Benjamins, J. W. *et al.* Genomic insights in ascending aortic size and distensibility. *EBioMedicine* **75**, 103783 (2022).
18. Tcheandjieu, C. *et al.* High heritability of ascending aortic diameter and trans-ancestry prediction of thoracic aortic disease. *Nat. Genet.* **54**, 772–782 (2022).
19. Solberg, S., Forsdahl, S. H., Singh, K. & Jacobsen, B. K. Diameter of the infrarenal aorta as a risk factor for abdominal aortic aneurysm: the Tromsø Study, 1994-2001. *Eur. J. Vasc. Endovasc. Surg.* **39**, 280–284 (2010).
20. Turkbey, E. B. *et al.* Determinants and normal values of ascending aortic diameter by age, gender, and race/ethnicity in the Multi-Ethnic Study of Atherosclerosis (MESA). *J. Magn. Reson. Imaging* **39**, 360–368 (2014).
21. Länne, T., Sonesson, B., Bergqvist, D., Bengtsson, H. & Gustafsson, D. Diameter and compliance in the male human abdominal aorta: influence of age and aortic aneurysm. *Eur. J. Vasc. Surg.* **6**, 178–184 (1992).
22. Whitcher, B. *et al.* Precision MRI phenotyping enables detection of small changes in body composition for longitudinal cohorts. *Sci. Rep.* **12**, 3748 (2022).
23. Bowman, A. W. & Kovács, S. J. Assessment and consequences of the constant-volume attribute of the four-chambered heart. *Am. J. Physiol. Heart Circ. Physiol.* **285**, H2027–33 (2003).
24. Carlsson, M. *et al.* Total heart volume variation throughout the cardiac cycle in humans. *Am. J. Physiol. Heart Circ. Physiol.* **287**, H243–50 (2004).
25. Santra, S. *et al.* Comparison of left ventricular mass in normotensive type 2 diabetes mellitus patients with that in the nondiabetic population. *J. Cardiovasc. Dis. Res.* **2**, 50–56 (2011).
26. Eguchi, K. *et al.* Association between diabetes mellitus and left ventricular hypertrophy in

a multiethnic population. *Am. J. Cardiol.* **101**, 1787–1791 (2008).

27. Foldyna, B. *et al.* Small whole heart volume predicts cardiovascular events in patients with stable chest pain: insights from the PROMISE trial. *Eur. Radiol.* **31**, 6200–6210 (2021).
28. Raffort, J. *et al.* Diabetes and aortic aneurysm: current state of the art. *Cardiovasc. Res.* **114**, 1702–1713 (2018).
29. Shah, A. D. *et al.* Type 2 diabetes and incidence of cardiovascular diseases: a cohort study in 1·9 million people. *Lancet Diabetes Endocrinol* **3**, 105–113 (2015).
30. Kuivaniemi, H. & Elmore, J. R. Opportunities in abdominal aortic aneurysm research: epidemiology, genetics, and pathophysiology. *Ann. Vasc. Surg.* **26**, 862–870 (2012).
31. Lederle, F. A., Parenti, C. M. & Chute, E. P. Ruptured abdominal aortic aneurysm: the internist as diagnostician. *Am. J. Med.* **96**, 163–167 (1994).
32. Macdonald, A. J., Faleh, O., Welch, G. & Kettlewell, S. Missed opportunities for the detection of abdominal aortic aneurysms. *Eur. J. Vasc. Endovasc. Surg.* **35**, 698–700 (2008).
33. Hardiman, G., Kastelein, R. A. & Bazan, J. F. Isolation, characterization and chromosomal localization of human WNT10B. *Cytogenet. Cell Genet.* **77**, 278–282 (1997).
34. Lyall, D. M. *et al.* Quantifying bias in psychological and physical health in the UK Biobank imaging sub-sample. *Brain Commun* **4**, fcac119 (2022).
35. Liu, Y. *et al.* Genetic architecture of 11 organ traits derived from abdominal MRI using deep learning. *Elife* **10**, (2021).
36. Ronneberger, O., Fischer, P. & Brox, T. U-Net: Convolutional Networks for Biomedical Image Segmentation. *Lecture Notes in Computer Science* 234–241 (2015) doi:10.1007/978-3-319-24574-4_28.
37. Grélard, F., Baldacci, F., Vialard, A. & Domenger, J.-P. New methods for the geometrical analysis of tubular organs. *Med. Image Anal.* **42**, 89–101 (2017).
38. Millard, L. A. C., Davies, N. M., Gaunt, T. R., Davey Smith, G. & Tilling, K. Software

Application Profile: PHESANT: a tool for performing automated phenome scans in UK Biobank. *Int. J. Epidemiol.* **47**, 29–35 (2018).

39. Carroll, R. J., Bastarache, L. & Denny, J. C. R PheWAS: data analysis and plotting tools for phenome-wide association studies in the R environment. *Bioinformatics* **30**, 2375–2376 (2014).
40. de Marvao, A. *et al.* Phenotypic Expression and Outcomes in Individuals With Rare Genetic Variants of Hypertrophic Cardiomyopathy. *J. Am. Coll. Cardiol.* **78**, 1097–1110 (2021).
41. Therneau, T. M. Survival Analysis [R package survival version 3.3-1]. (2022).
42. Bycroft, C. *et al.* The UK Biobank resource with deep phenotyping and genomic data. *Nature* **562**, 203–209 (2018).
43. Loh, P.-R. *et al.* Efficient Bayesian mixed-model analysis increases association power in large cohorts. *Nat. Genet.* **47**, 284–290 (2015).
44. Bulik-Sullivan, B. K. *et al.* LD Score regression distinguishes confounding from polygenicity in genome-wide association studies. *Nat. Genet.* **47**, 291–295 (2015).
45. Integrating common and rare genetic variation in diverse human populations. *Nature* **467**, 52–58 (2010).
46. Yang, J. *et al.* Conditional and joint multiple-SNP analysis of GWAS summary statistics identifies additional variants influencing complex traits. *Nat. Genet.* **44**, 369–375 (2012).
47. Smedley, D. *et al.* The BioMart community portal: an innovative alternative to large, centralized data repositories. *Nucleic Acids Res.* **43**, W589–98 (2015).
48. Loh, P.-R., Kichaev, G., Gazal, S., Schoech, A. P. & Price, A. L. Mixed-model association for biobank-scale datasets. *Nat. Genet.* **50**, 906–908 (2018).
49. Kundaje, A. *et al.* Integrative analysis of 111 reference human epigenomes. *Nature* **518**, 317–330 (2015).
50. ENCODE Project Consortium. An integrated encyclopedia of DNA elements in the human

genome. *Nature* **489**, 57–74 (2012).

51. GTEx Consortium. Genetic effects on gene expression across human tissues. *Nature* **550**, 204–213 (2017).
52. Fehrmann, R. S. *et al.* Gene expression analysis identifies global gene dosage sensitivity in cancer. *Nat. Genet.* **47**, (2015).
53. Pers, T. H. *et al.* Biological interpretation of genome-wide association studies using predicted gene functions. *Nat. Commun.* **6**, 1–9 (2015).
54. Storey, J. D. & Tibshirani, R. Statistical significance for genomewide studies. *Proc. Natl. Acad. Sci. U. S. A.* **100**, (2003).
55. Giambartolomei, C. *et al.* Bayesian test for colocalisation between pairs of genetic association studies using summary statistics. *PLoS Genet.* **10**, e1004383 (2014).
56. Zhou, W. *et al.* Scalable generalized linear mixed model for region-based association tests in large biobanks and cohorts. *Nat. Genet.* **52**, 634–639 (2020).
57. Zhao, J. H. Gap: Genetic analysis package. *J. Stat. Softw.* **23**, (2007).
58. Wickham, H. *ggplot2: Elegant Graphics for Data Analysis*. (Springer, 2016).

Supplementary Figures

SF1: Phenome-wide study of self-reported exposures and health outcomes

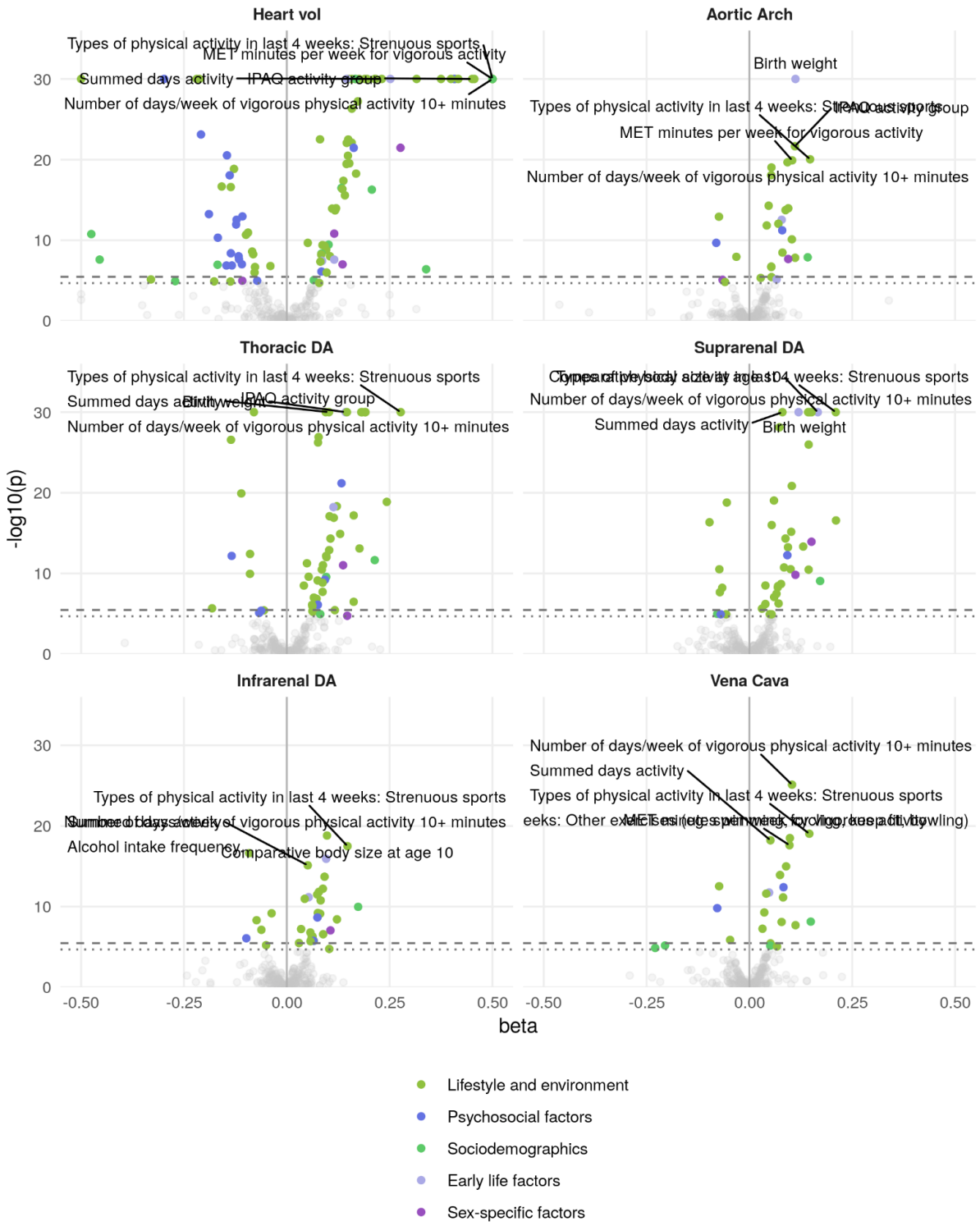

SF2: Phenome-wide plot of Lifestyle and History

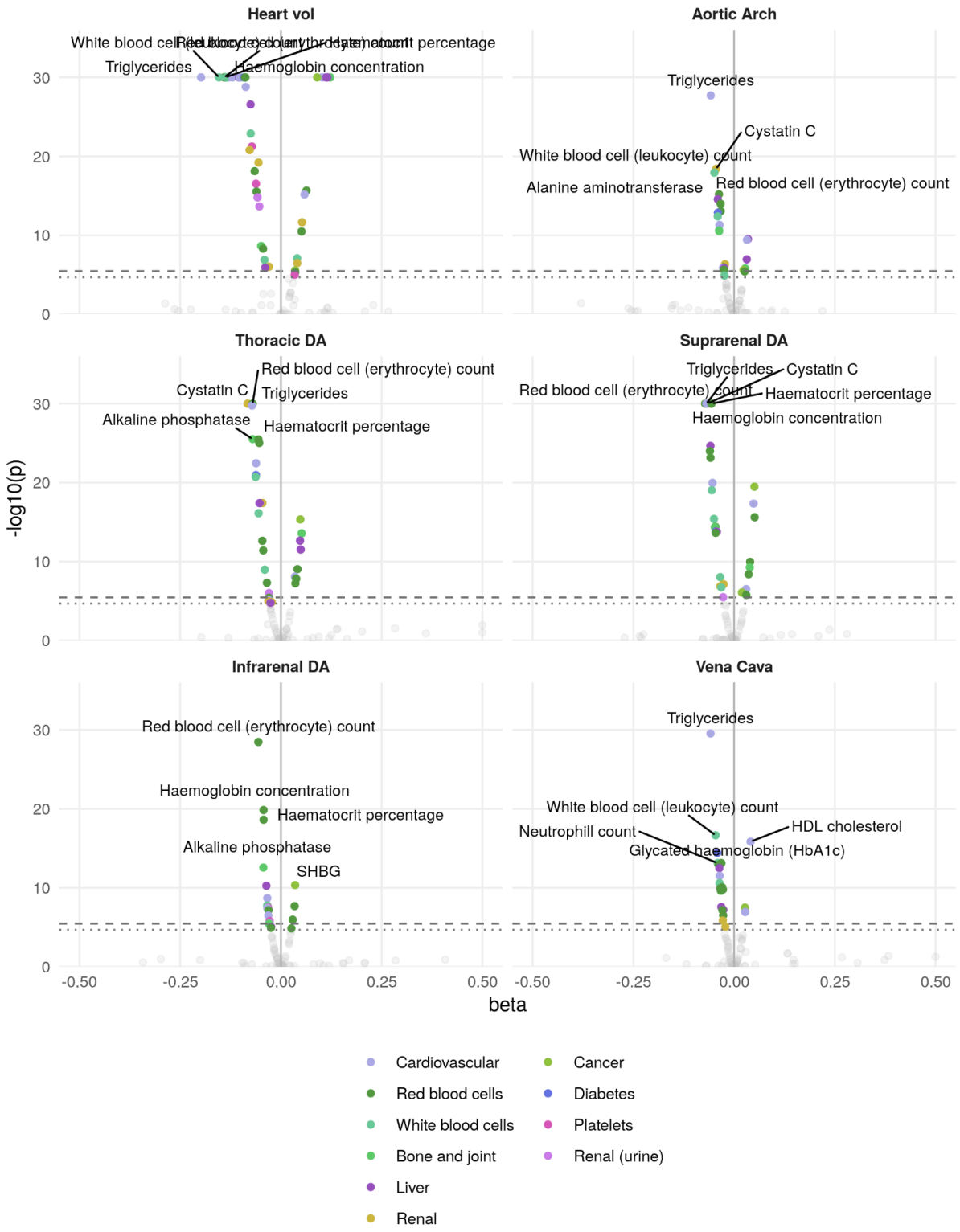

SF3: Phenome wide plot of blood biomarkers

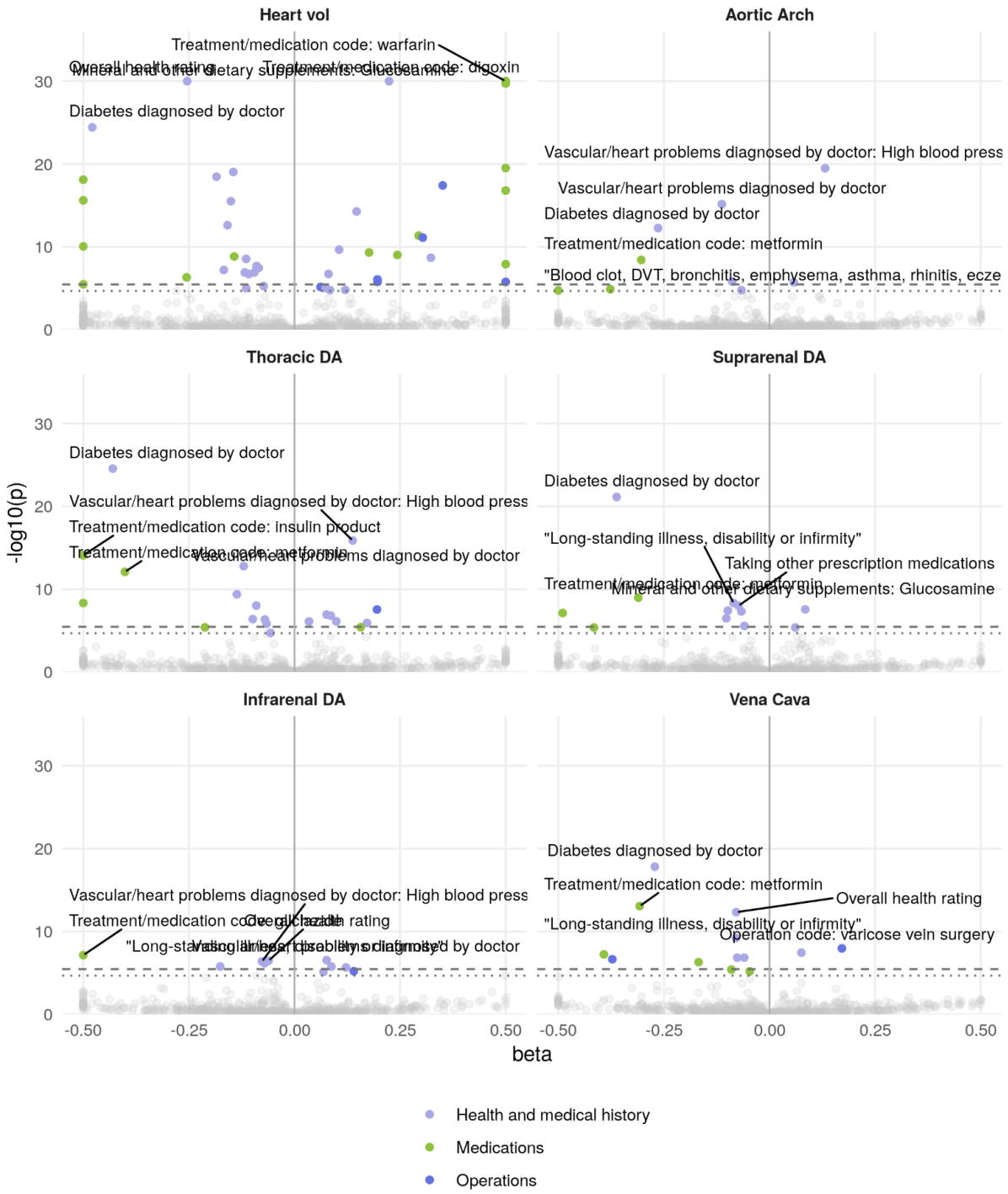

SF4: Phenome-wide plot of self-reported medical history, operation codes, and health outcomes

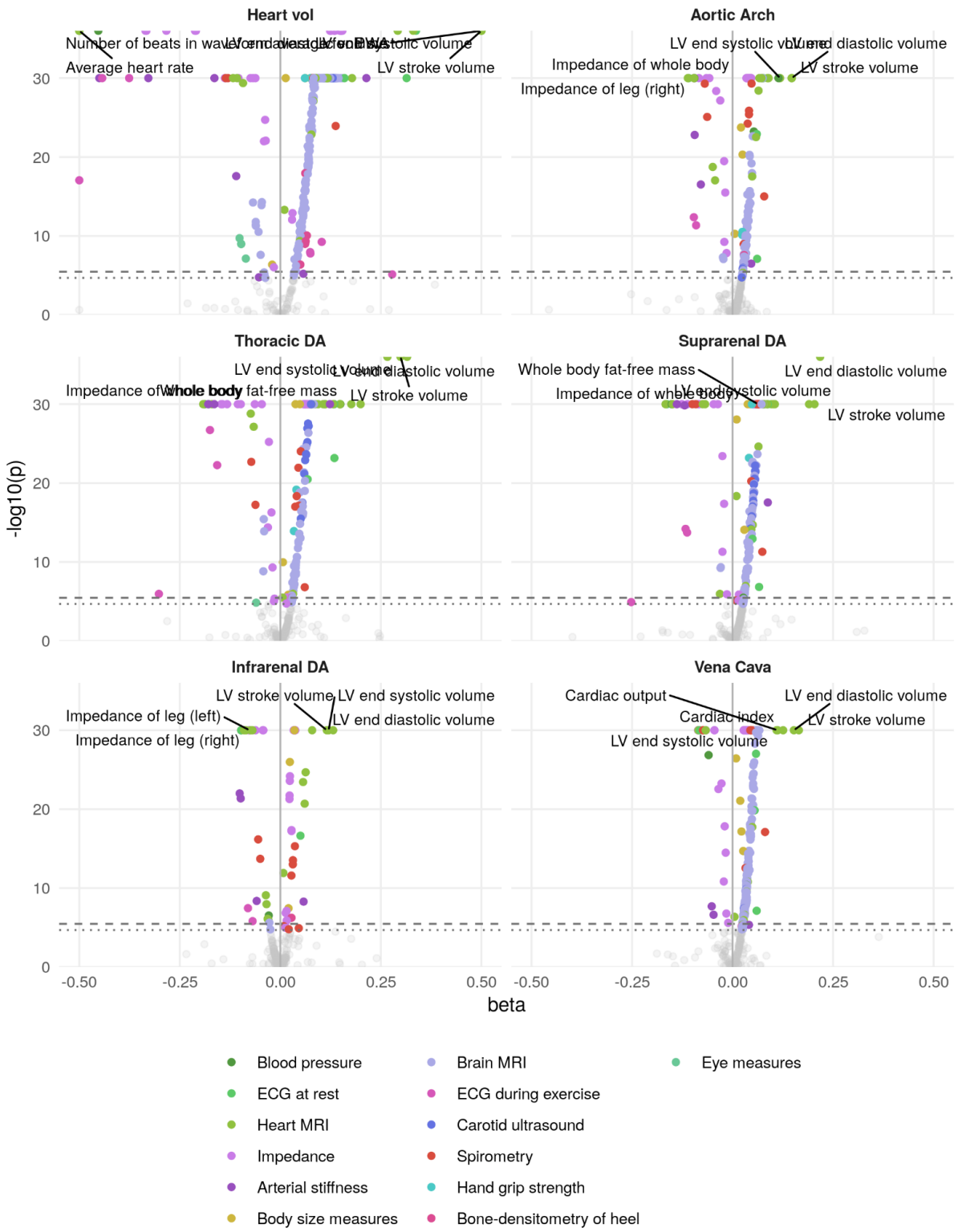

SF5: Phenome-wide plot of physical measures

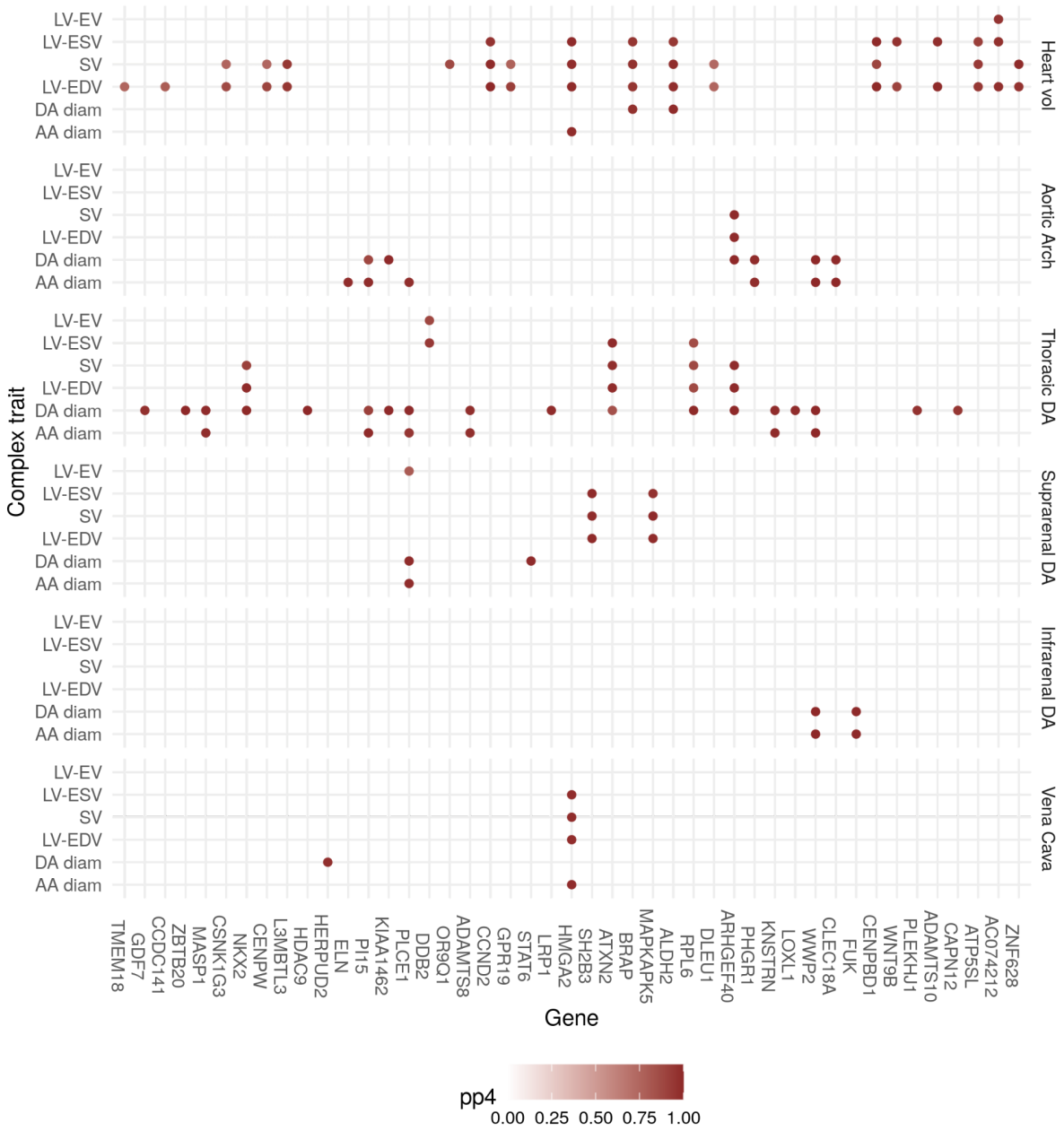

SF6 : Colocalizing loci with other MRI derived traits

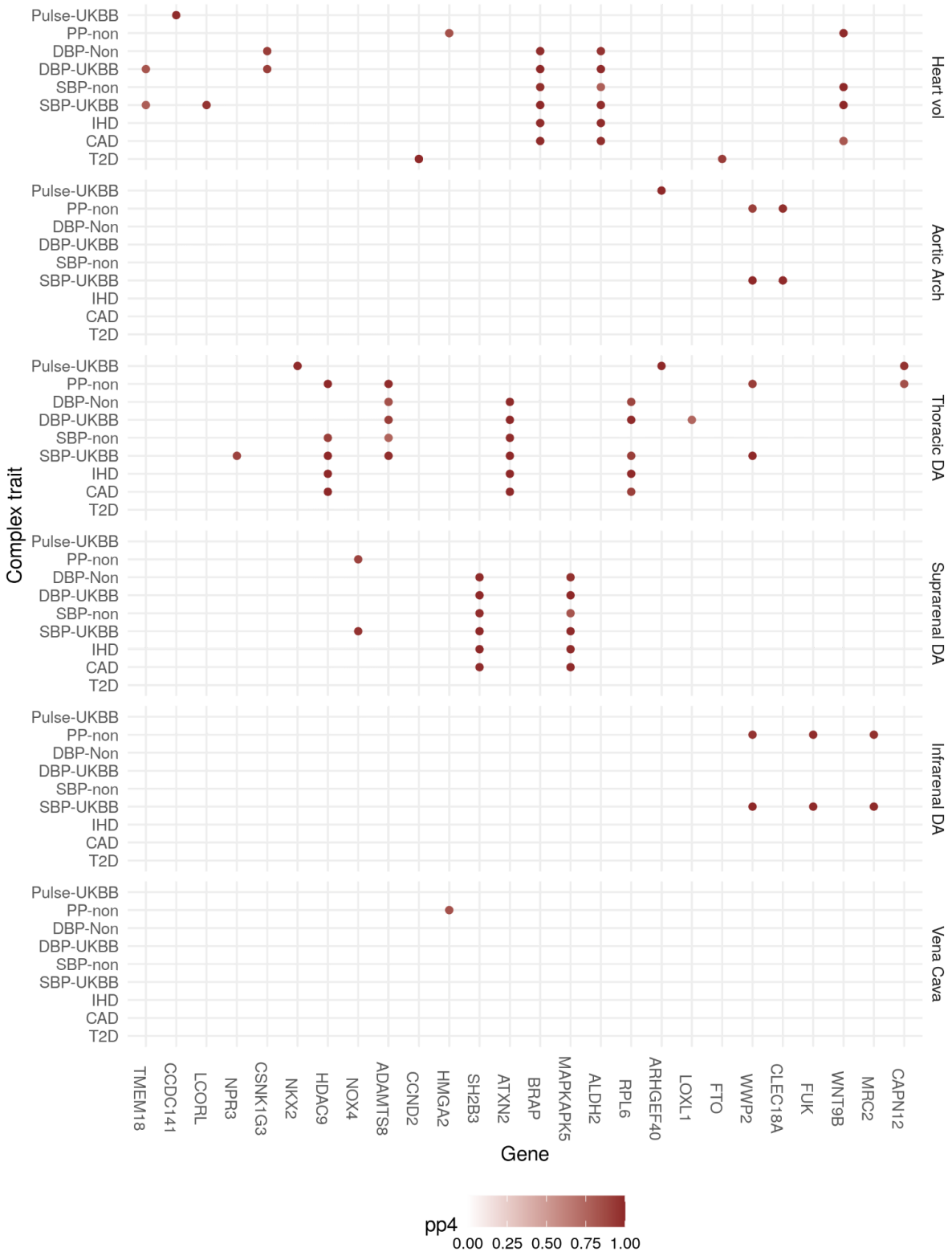

SF7: Colocalisation with cardiovascular complex traits. Colocalisations with PP4 > 0.7 shown. Two blood pressure studies are used - one from the UK Biobank, and one from a non-UK Biobank sample from the GERA study. CAD: Coronary artery disease. IHD:

Ischaemic heart disease. T2D: Type 2 diabetes.

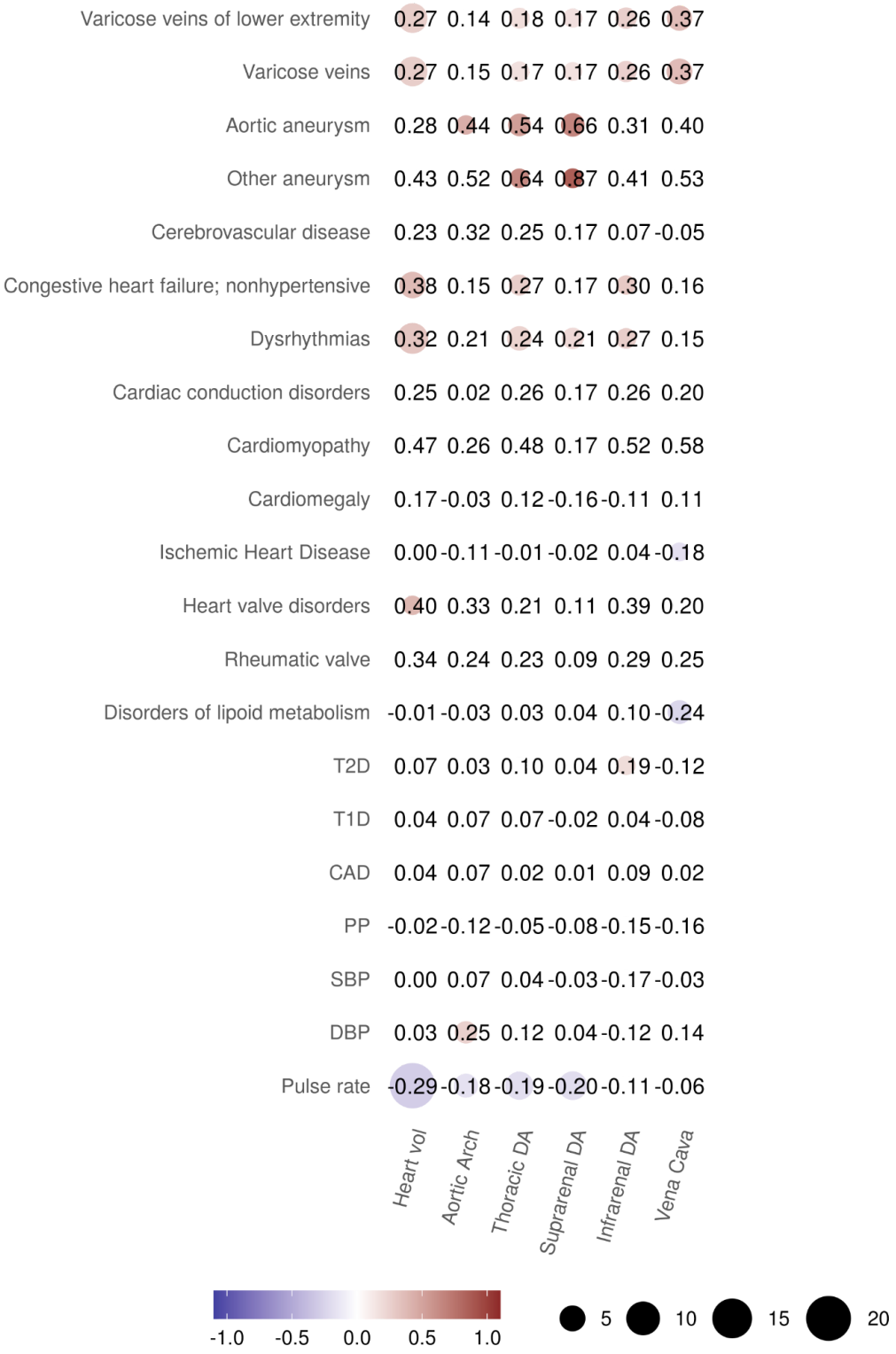

SF8: Genetic correlation with an expanded range of cardiovascular traits.

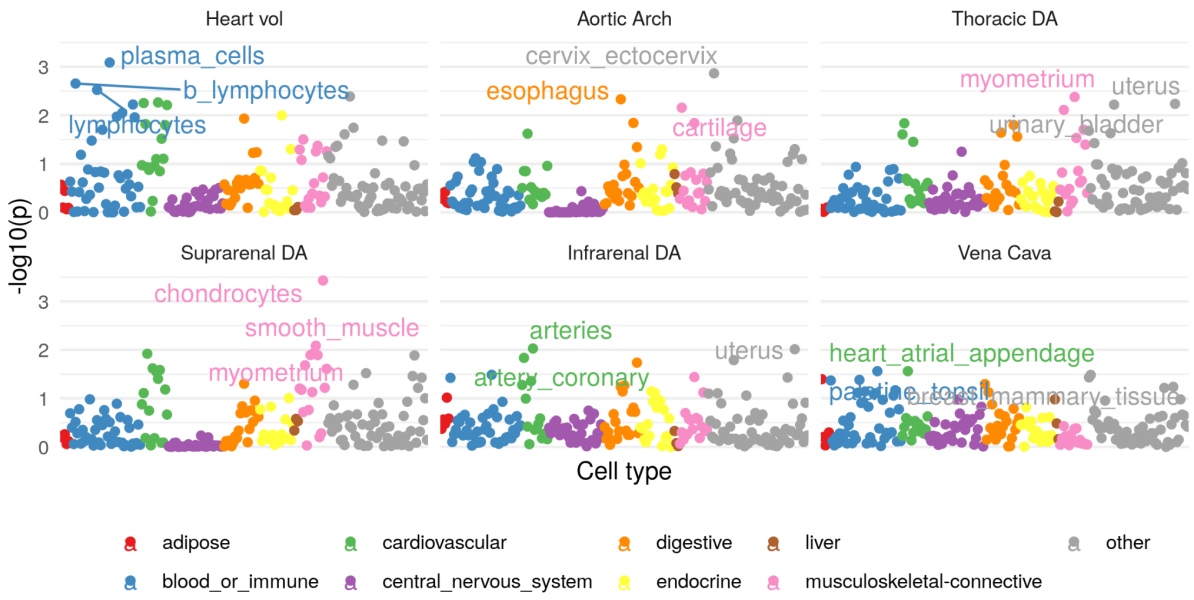

SF9: Gene expression heritability enrichment

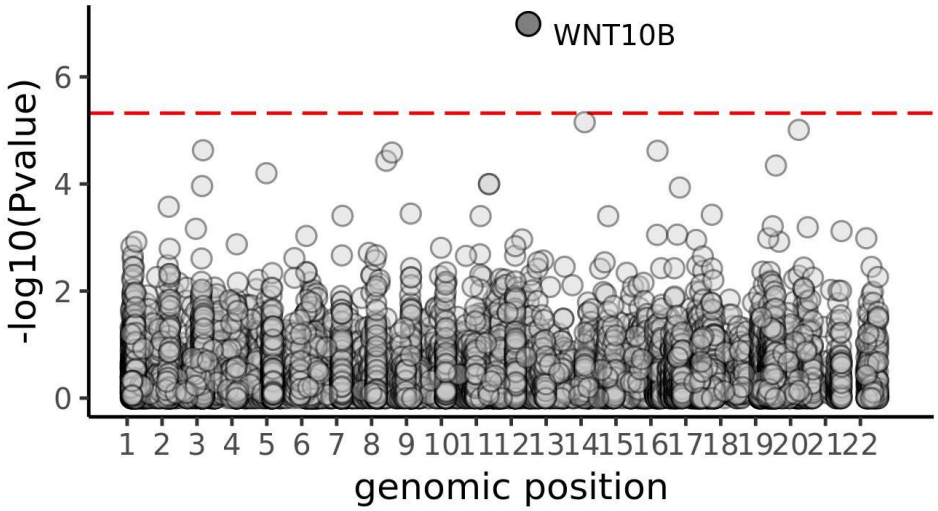

SF10: Rare variation in *WNT10B* is associated with heart volume. Rare variant association study of heart volume identified *WNT10B* ($p_{SKAT\text{-}O}$=1.0e-7). The Bonferroni significance line is shown in red.

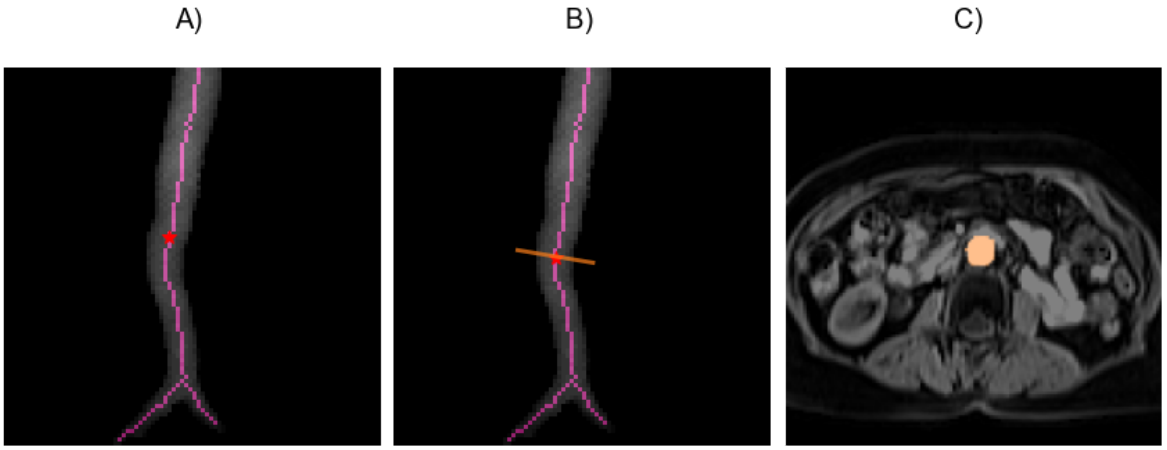

SF11: Placement of orthogonal plane along the aorta. A) Aorta segmentation, skeleton and landmark. B) Tangent to the aorta at the landmark. C) Extracted orthogonal plane.

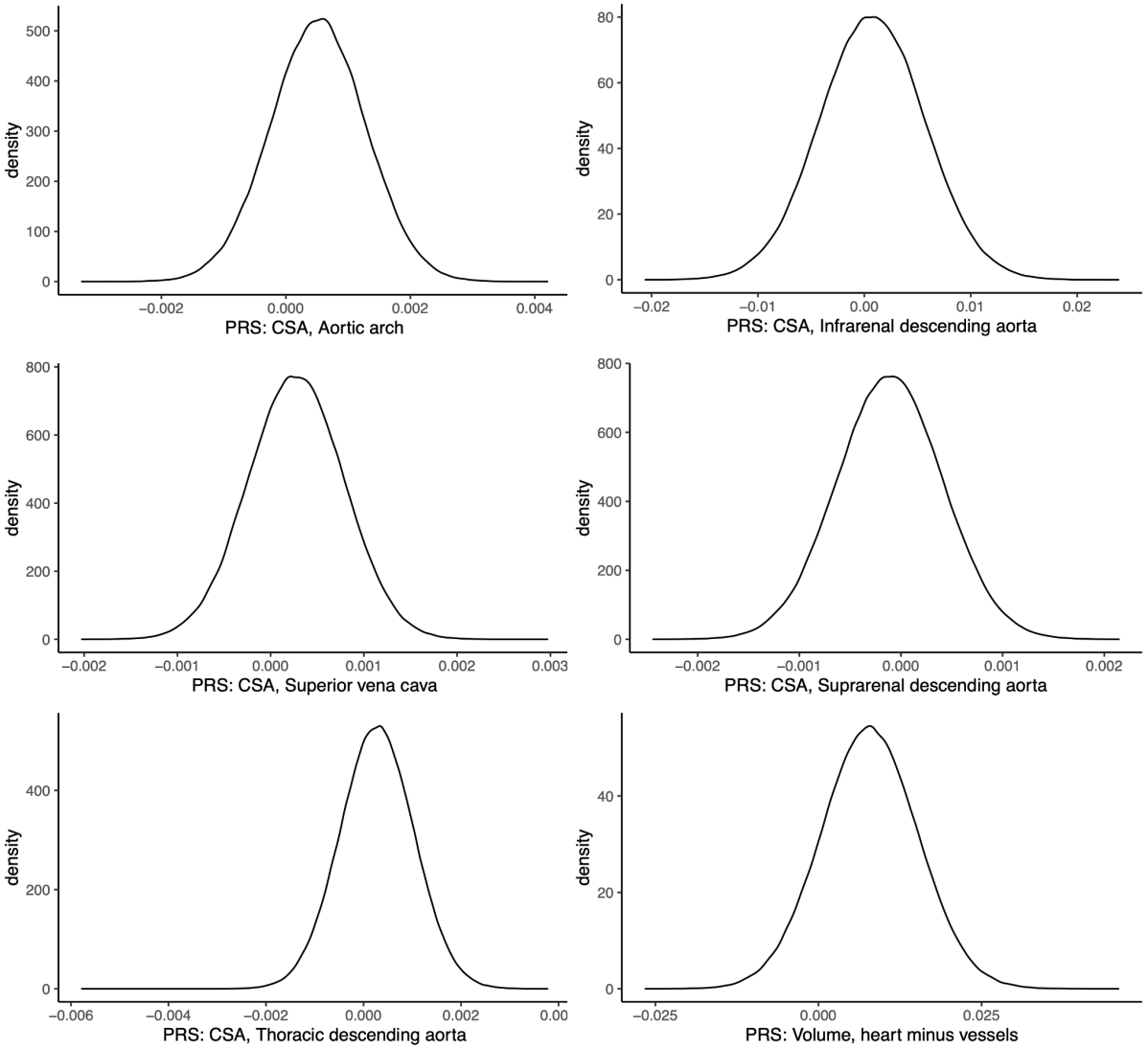

SF12: Polygenic risk score (PRS) distributions for six IDPs in the UK Biobank: Aortic arch, Infrarenal descending aorta, Superior vena cava, Suprarenal descending aorta, Thoracic descending aorta, and Heart volume minus vessels. CSA, cross-sectional area.

Supplementary tables

https://docs.google.com/spreadsheets/d/1Y4OBCW4dRDEIDpJmt4m7L0DJGNiY3BY0sUgVpeUxnpE/

ST1: Summary statistics of image-derived phenotypes (IDPs) stratified by sex. IDPs are measured as cross-sectional areas in mm^2 (aortic arch, thoracic descending aorta, suprarenal descending aorta, infrarenal descending aorta, superior vena cava) or as volume in mm^3 (heart).

ST2: Summary statistics of image-derived phenotypes (IDPs) stratified by sex and percentiles.

ST3: Regression of IDP values against age, adjusted for scan date, scan time, study centre, height and weight.

ST4: Results from disease phecode associations

ST5: Results from phenome-wide associations

ST6: Summary statistics of aorta image-derived phenotypes (IDPs) stratified by sex and aneurysm status. We determined aneurysm based on IDPs either if infrarenal CSA > $700mm^2$ (3cm diameter) [12] or infrarenal CSA > mean + 2 SD.

ST7: Heritability and standard errors of each IDP

ST8: Lead variants at each locus with each trait. pv=pvalue. pp=posterior probability that this is the causal variant.

ST9: GTEx Colocalisation. Posterior probability of colocalisation of eQTLs in cardiovascular tissue.

ST10: Polygenic risk score (PRS) training across a range of p-value thresholds from p = 1e-8 to p = 0.1. R^2 for full model includes adjustment for age, age^2, sex, standardized scan time and date, imaging center, and genotyping platform.

ST11: Polygenic risk score cox proportional hazard models

ST12: Definitions for disease outcomes for aneurysm, major adverse cardiovascular events (MACE) and varicose veins. Field 20002: Self-reported non-cancer illness; ICD10: International Classification of Disease 10th edition.

ST13: LDSC intercept

ST14: Genome-wide association studies used To identify cardiovascular disease traits potentially sharing the genetic basis with our IDPs